J. Fluid Mech. (1986), *vol.* 173, *pp.* 557–594
Printed in Great Britain

The intrusion of fluid mechanics into geology

By HERBERT E. HUPPERT

Department of Applied Mathematics and Theoretical Physics, University of Cambridge, Silver Street, Cambridge CB3 9EW, UK

(Received 26 March 1986)

During the last few years, a number of fluid dynamicists, often in collaboration with geologists, have been investigating problems suggested by geology and creating the new field of geological fluid mechanics. The research has uncovered many new fluid-mechanical phenomena and the studies have ranged widely over theoretical contributions, laboratory experiments and confirmatory field observations. This paper presents an overview of part of the field, with a strong emphasis on the novel fluid-mechanical concepts. The presentation includes discussion of some of the effects of cooling and crystallization and the resulting convective motions, the flow of gravity currents at both high and low Reynolds number, and the erosion of solid retaining walls by hot, turbulent flows.

1. Introduction

The last few years have seen major developments in the application of fluid mechanics to problems in the geological sciences. The range and depth of understanding are now sufficient that the discipline warrants the distinct name of geological fluid mechanics (GFM). A major part of the subject, which will be concentrated upon in this review, is concerned primarily with the various motions of the fluid material that upon solidification becomes the rocks that make up the Earth. The study of GFM involves the investigation of many novel fluid-mechanical phenomena motivated by a wide range of geological applications. Scientists working in the subject have already opened up a number of new areas in fluid mechanics and, at the same time, have changed the way geologists think about and interpret rock suites, both beneath and on the Earth's surface. There is every indication that the subject will continue to expand and provide interesting, solvable problems for applied mathematicians, fluid dynamicists and geologists.

This paper presents a fluid-dynamicist's view of part of the new subject and is aimed at explaining the novel concepts to those familiar with the ideas of fluid mechanics. It inevitably focuses on the investigations in which I have been involved, though it also describes the work of others. New, fundamental principles are highlighted, while the reader is referred to the original papers for details. Some of the material has appeared recently in the geological literature, but the presentation here is rather different, in part because the fluid mechanics is stressed and the geological applications are only briefly described.

The next section surveys the geological background that defines the subject. I then attempt to bring out some unifying principles by analysing three different situations in the following three sections. As an aid to the reader of a rather long paper, however, I should point out that the presentation of each of these three sections is independent and that each can be read on is own. From a fluid-mechanical point of view, the sections deal with: §3 cooling, crystallization and resultant evolution of a two-layer

aqueous system; §4 spreading of a viscous gravity current; and §5 flow of a hot, turbulent density current over an erodible bed.

From a geological viewpoint, the sections deal with aspects of: §3 evolution of a magma chamber beneath a volcano; §4 creation of a volcanic lava flow in the crater of a volcano; and §5 flow of lava some 3000 million years ago with the resultant deposition of a major fraction of the world's supply of nickel accessible to man.

A more qualitative final section briefly describes other areas of the subject and concludes with a few remarks about future developments.

2. Geological background

A description of GFM commences most conveniently with a discussion of the formation of melt from solid rock within the Earth. Melting is a consequence of the variation of pressure, and hence melting temperature, with depth. At specific places in the Earth's mantle, explicitly beneath the mid-ocean ridges, hot solid rock is convected towards the Earth's surface in response to large-scale global processes. The temperature of the rising solid rock decreases less rapidly that its melting temperature. A depth is thus reached at which partial melting commences, and above that depth the proportion of melt within the multicomponent rock increases. At other places cool, solid rock near the Earth's surface is downthrust or subducted into the mantle. The temperature of the rock increases with depth as it descends, and a point is reached where it also can start to melt.

The melt is generally less dense than the surrounding solid and percolates upwards through a series of contorted channels by a process known as compaction (McKenzie 1984, 1985). The details of this flow are not yet totally understood. Marsh (1978) has considered the quantitative consequences of different flow models and calculations have been presented for the propagation of a two-dimensional, fluid-filled crack driven by buoyancy in an elastic medium (Spence & Turcotte 1985; Spence, Sharp & Turcotte 1986). It has also been suggested that the melt may migrate in solitary-wave-like batches, which are sometimes called magmons (Richter & McKenzie 1984; Scott and Stevenson, 1984; Scott, Stevenson & Whitehead 1986). It appears that, somehow, the melt often accumulates in large storage reservoirs, known as magma chambers ('magma' being the geologists' word for molten or partially molten rock within the Earth; upon extrusion at the Earth's surface it is called 'lava'). These chambers differ in size from a fraction of a cubic kilometer to a few thousand cubic kilometers (a few tens of kilometers in horizontal extent and a few kilometers in the vertical). Magma may repose in one or more such chambers during its ascent towards the Earth's surface. The repose time for a particular fluid element can range from as little as a few hours through to effectively forever, the latter limit occurring if the magma cools sufficiently while in the chamber to solidify there. In general, however, the repose time stretches from years to thousands of years or much more, during which time the magma cools, partially solidifies and evolves chemically and physically. Fluid-mechanical thinking is making a large contribution to understanding the various processes that occur in magma chambers. Part of the work along this line will be described in §§3 and 6.

From the magma chamber, magma can rise to the surface of the Earth, through long fissures or circular conduits in the crust, and either becomes part of the output of an explosive volcanic eruption, which can be quite violent, or is more gently extruded onto the Earth's surface as lava. An explosive eruption may involve regimes of supersonic gas dynamics because the eruption velocities of the gas/magma mixture

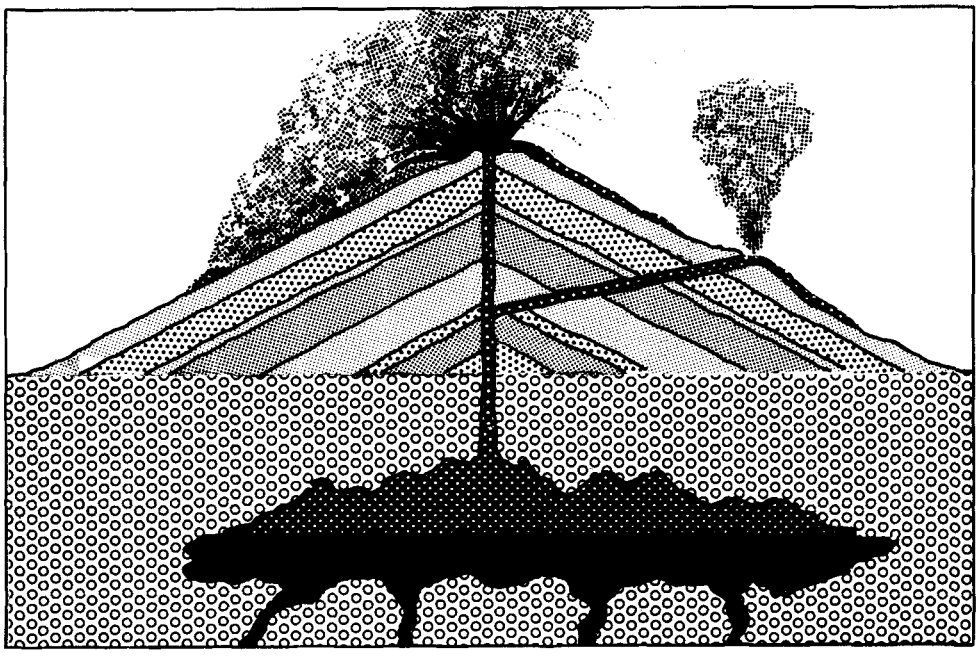

FIGURE 1. An artist's sketch of a typical cross-section through a volcano and magma chamber. Magma flows from depth into the stratified chamber before coming to the surface and being erupted. Plumes rise from the vents which also discharge lava and heavy, ash-laden pyroclastic flows.

can be as high as Mach 3 (Kieffer 1977; Wilson, Sparks & Walker 1980). The vent acts as a Laval nozzle with an interesting difference – the force of the flow is sufficient to blow out the surrounding rocks and to mould the conduit. This interaction between the flow and the shape of the nozzle plays an important role in determining the details of the eruption.

Above an erupting volcano there is generally an explosive eruptive column, or plume of hot ash and gases, which can penetrate up to 45 km into the atmosphere. Some of the fluid-mechanical phenomena associated with such a column are described in §6. The flow of molten rock (now lava) on the Earth's surface – either on land, or under the ocean – accompanies many eruptions. The rate of advance of the lava flow, its rate of cooling and solidification and the lateral extent of the final state are all interesting and, from a practical point of view, important problems. The fluid mechanics involved in some aspects of lava flow is described in §§4 and 5.

A pictorial summary of all these processes is contained in an artist's sketch of a typical cross-section through a volcano (figure 1). Many of the situations described above can be seen in this figure.

It would be impossible to delimit rigidly the areas of interest which make up GFM. The above areas constitute a part of the mainstream of the subject. Other areas might quite reasonably be included, such as: the propagation of mud flows, which were so devastating after the Mount St. Helens and Nevado del Ruiz eruptions; the geology of sedimentary basins and the associated formation of oil; the activation of geothermal systems; parts of sedimentary geology, including the formation and propagation of sand dunes; and possibly the dynamics of plate tectonics and the motions of the liquid outer core, though these have historically been considered geophysical rather than geological topics. It is clear that buoyancy-driven flows, often

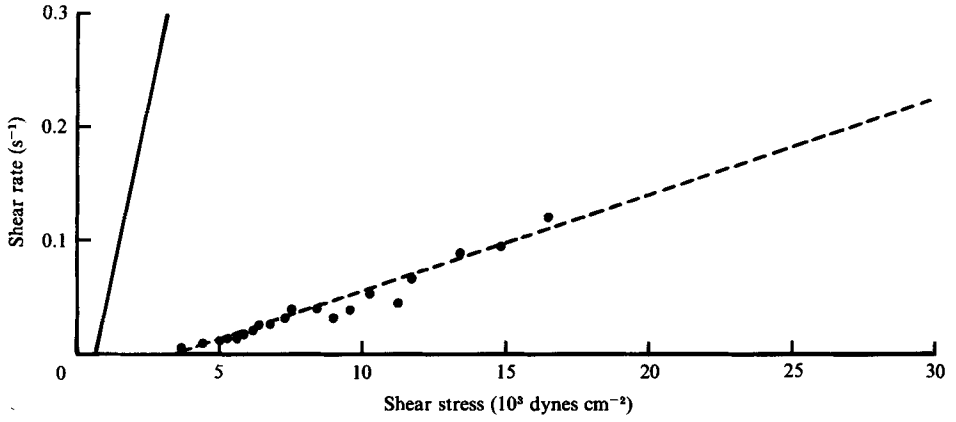

FIGURE 2. The measured rheology of lava in the Makapouhi lava lake (——) and in a flow on Etna (– – –).

in association with solid/liquid phase changes, are essential ingredients in many of the problems. Other ingredients are often dictated by the geological applications.

Physical and chemical properties

Detailed fluid mechanics depends heavily on the physical properties of the fluid under consideration. The two physical properties which are particularly important here are rheology and density. *In situ* measurements have not yet been carried out on magmas, but there are many field observations of lavas. Lava lakes, such as those of Hawaii, and lava flows from erupting volcanoes, particularly those from Mount Etna in Italy, have been the sites of extensive rheological and densimetric measurements. Further knowledge has been obtained from laboratory measurements on either molten rocks or synthetic silicate melts. From all these measurements, geologists have devised empirical formulae that relate stress and rate of strain, and give effective viscosity and density as functions of composition, temperature and, occasionally, pressure.

It is generally believed that magmas which have rather low concentrations of both crystals and gas bubbles behave like Newtonian fluids. Once the magma has cooled somewhat and crystallized extensively, however, it can display non-Newtonian characteristics. Figure 2 presents two sets of rheological measurements made in the Makapouhi lava lake on Hawaii and in a lava flow on Etna. In both measurements, a yield strength is evident, of approximate magnitude of 10^3 dynes cm^{-2} in Makapouhi and 4×10^3 dynes cm^{-2} on Etna. For stresses well above these values, the measurements suggest that the lavas are reasonably Newtonian. While some non-Newtonian behaviour may be important in lava flows, my own belief (which is shared by many others) is that in many situations of lava motion, the shear stresses well exceed the yield stress and that the subject can be advanced at the moment by analysing responses based on the assumption of Newtonian fluid mechanics. Subsequent refinement may be required, but at present many fundamental, though basically Newtonian, aspects remain to be elucidated.

On the assumption that magmas and lavas with a given temperature and composition can be characterized by a specific viscosity, geologists derive empirical plots of melt viscosity for particular magmas as they cool. Such a plot is presented in figure 3. Two important facts are obvious. First, viscosity is strongly affected by

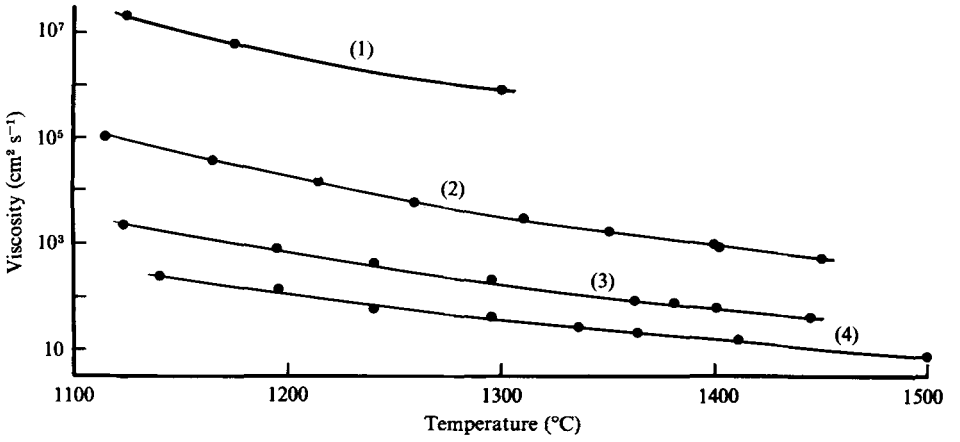

FIGURE 3. The viscosity of a magma as a function of temperature: (1) rhyolite with 73.4 % SiO_2; (2) andesite with 60.7 % SiO_2; (3) basalt from Oregon USA with 50.7 % SiO_2; (4) basalt from the Galapagos with 46.1 % SiO_2. (From Murase & McBirney 1973.)

rather slight differences in composition. Secondly, the viscosity increases strongly as the temperature decreases. The former variation is an essential ingredient in many theoretical models of magma motion, though the latter has not been incorporated to the same extent. The shear viscosity of melt plus crystals μ_P is often obtained empirically from the viscosity of the pure melt μ_M by

$$\mu_P = \mu_M(1-1.67x)^{-2.5}, \tag{2.1}$$

where x is the volume fraction of crystals (Marsh 1981). As the crystal content increases, the behaviour of the magma increasingly departs from that predicted by using Newtonian concepts, and for a crystal content in excess of approximately 0.55 magma ceases to flow and effectively becomes a solid. However, when the crystal content is less than about a third, the departures are generally relatively small.

The density of a magma or lava can vary significantly as it cools and crystallizes. This variation has important consequences for the form of convective motion produced. Figure 4 presents the density as a function of temperature of the pure, residual melt (fluid *without* crystals) for two different magma types. (The chemical differences between these magmas are discussed below.) Also graphed are the corresponding bulk densities (fluid *plus* crystals). For both sets of curves, significant variations occur both as a function of temperature for a particular magma and between different magmas. The inclusion of even a small amount of dissolved water can also lead to fairly large changes in density. Some of the fluid-mechanical implications of dissolved and exsolved water in magmas injected into magma chambers have been investigated by Huppert, Sparks & Turner (1982*b*) and Turner, Huppert & Sparks (1983) and will be mentioned in the next secton.

Of course, much more could be written about the physical properties of silicate melts. The above is sufficient, however, to act as a foundation for the various particular investigations discussed in the following sections. Readers who seek more knowledge might refer to Shaw (1969), Nelson & Carmichael (1979), McBirney & Murase (1984) and Sparks & Huppert (1984).

For readers with little background in geology, the nomenclature of magmas and the resultant rocks, which is based on their chemical compositions, can obscure the fundamental concepts. I will attempt to use the least amount of jargon commensurate

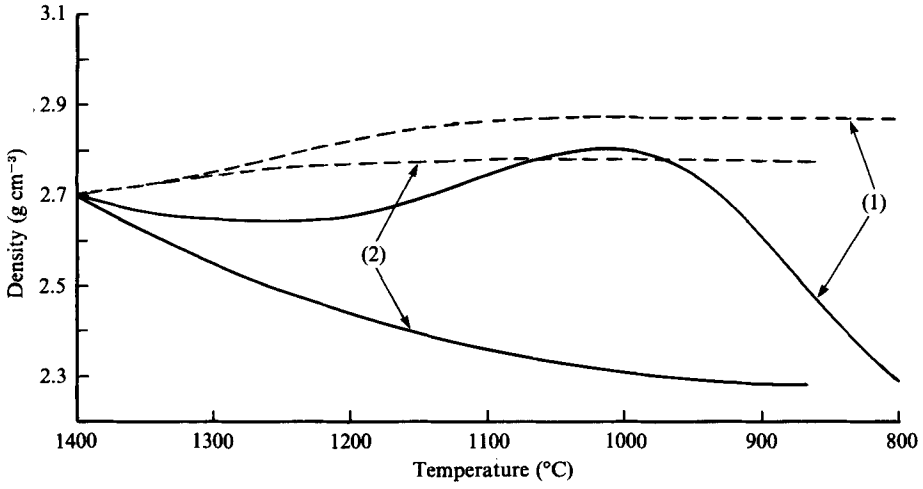

FIGURE 4. Density as a function of (decreasing) temperature for two different magma types known as (1) tholeiitic and (2) calcalkaline magmas. The solid curves represent the density of the liquid magma and the dashed curves the bulk density of magma plus crystals.

with highlighting the main features of volcanism on the Earth. By far the dominant magma type is *basalt*, which is formed by melting of the Earth's mantle. Basalts are composed of about 50 % SiO_2 with the oxides of the elements Al, Fe, Ca, Mg and Na constituting most of the remainder. Basalt magmas within the Earth have temperatures between 1100 and 1250 °C, densities between 2.60 and 2.75 g cm^{-3} and viscosities between 30 and 1000 $cm^2\ s^{-1}$. *Rhyolite* magmas are much richer in silica – containing between 70 and 75 % SiO_2 – while the remainder consists mainly of the oxides of Al, Na and K with little Fe, Mg or Ca. They typically form by melting of the continental crust. They have temperatures between 700 and 1000 °C, densities of about 2.3 g cm^{-3} and viscosities between 10^4 and 10^{12} $cm^2\ s^{-1}$. The variation in viscosity is due principally to the effects of temperature and small amounts of dissolved water in melts rich in SiO_2. For example, dissolving 4 % by weight of water into a rhyolite can reduce the viscosity by several orders of magnitude. *Andesite* magmas are intermediate in chemical composition between basalt and rhyolite and usually have intermediate temperatures and physical properties. Andesites occur frequently in volcanoes above subduction zones, such as Mount St. Helens in USA and Nevado del Ruiz in Columbia.

3. The evolution of a replenished two-layer system

The first situation to be analysed in this section is described diagramatically in figure 5. Consider a hot, heavy layer of fluid rapidly introduced beneath a cooler, lighter layer. The fluid that makes up the lower layer may be an aqueous salt solution, such as KNO_3, as has been used in our laboratory experiments, or any multi-component melt that crystallizes as it cools. The first point to note is that it is possible to have a hotter, yet heavier, layer because of the compositional influence on the density of the lower layer. The general observation that compositional effects on density almost always outweigh thermal effects can lead to many new phenomena.

Because the lower layer is hotter than the upper layer, it cools by transferring its heat to the upper layer. We shall assume that the system is insulated so that no heat is lost to the surroundings. As the lower layer cools, it can reach a point where one

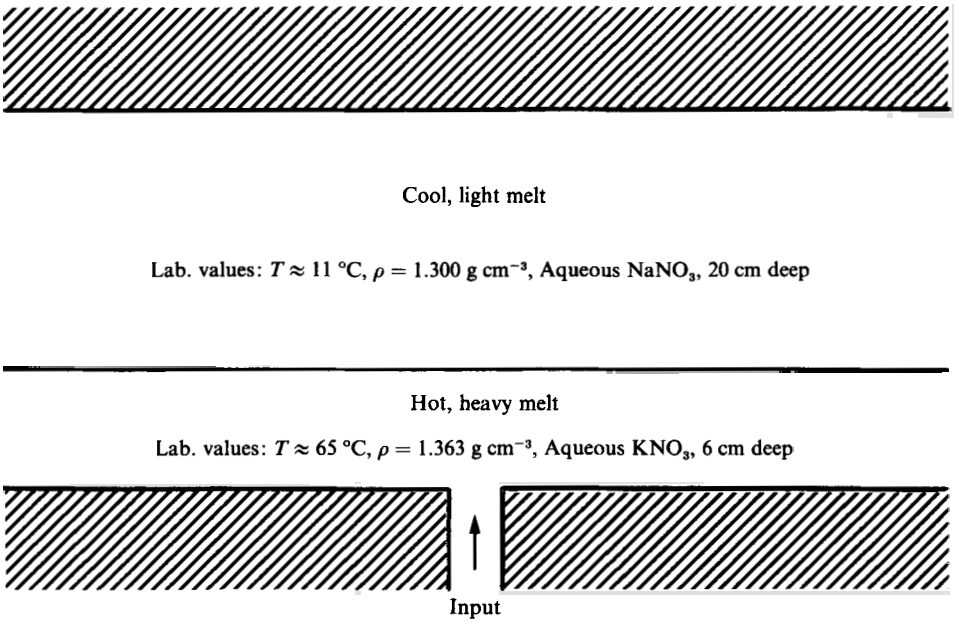

FIGURE 5. A diagrammatic sketch of a hot, heavy layer beneath a cooler, less dense layer.

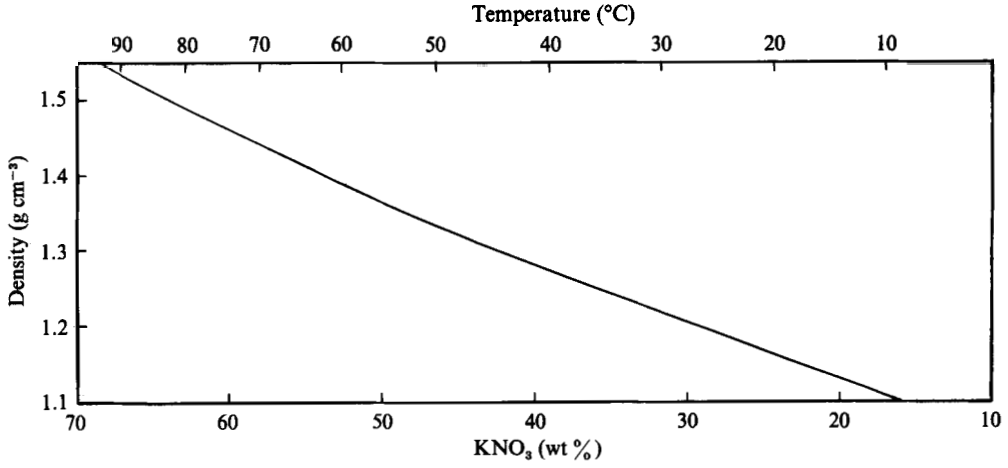

FIGURE 6. The density of saturated KNO_3 as a function of either composition or temperature.

component of the melt begins to crystallize. The evolution thereafter depends very much on the density of the residual liquid. Often, and in all the laboratory experiments we have conducted, the density of the liquid left behind after crystallization decreases as the temperature decreases. This is demonstrated in figure 6 which presents the density as a function of temperature for (saturated) aqueous KNO_3. This decrease contrasts with the more familiar increase of density with decreasing temperature in a non-crystallizing system and provides many novel effects.†

We shall assume, as is appropriate for most laboratory and natural situations, that

† An account of the influence of variations of the density of the residual liquid with temperature and composition in a number of magmatic problems is given by Sparks & Huppert (1984).

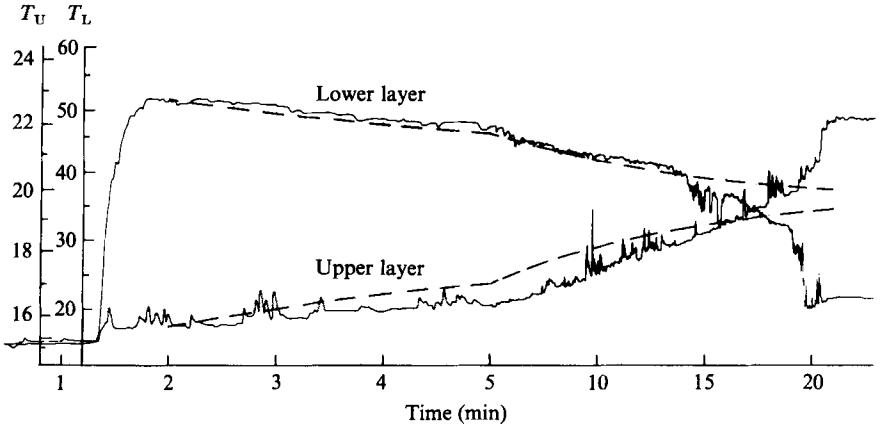

FIGURE 8. Temperature of the lower layer T_L and the upper layer T_U as a function of time (plotted on a scale which changes after 5 min). The solid curves represent the experimental measurements and the dashed lines are the theoretical predictions. Note that the temperature scales used for the upper and lower layers are different and that after the overturn, which commences at approximately 18 min, the temperatures equilibrate to the same value.

the Rayleigh numbers are well in excess of those required to make the motion in each of the two layers turbulent. A paper-thin interface separates the two layers, and strong thermal transfer, with negligibly small compositional transfer, takes place across the double-diffusive interface. As the temperature of the lower layer decreases, so does the liquid density, until a point can be reached at which the density of the liquid in the lower layer equals that in the upper layer. The fluid of the lower layer then rises into the upper layer and, if the viscosities of the two layers are sufficiently small, mixes intimately with it. This process is depicted in figure 7 (Plate 1).

For simple salts the transfer rates across the interface are known and the temperature history of either layer, and in particular the lower layer, can be determined. Figure 8, taken (with but slight alteration) from Huppert & Turner (1981), presents the temperature of the upper and lower layers as functions of time from one of our experiments. Also included in the figure are the predicted temperatures, which were calculated, as indicated in Huppert & Turner (1981), from the known heat transfer rates.

While the temperatures of the two layers can be quite accurately predicted as functions of time, the liquid density as a function of temperature is essentially unpredictable. Figure 9 displays measurements of density and temperature of the lower layer for one of our experiments. The dashed line is the saturation curve, taken from Washburn (1929) (and has been substantiated by our own direct measurements). The lower layer commences on the undersaturated side of this curve and migrates towards it (with density increasing with decreasing temperature, as is usual). It crosses the curve, becomes supersaturated and does not form any crystals until the point A in the figure. The degree of supersaturation, here approximately 5 °C, depends on the purity of the water, the explicit chemicals, the container and the procedures of the experiment. Much higher, or lower, supersaturations can be readily obtained (Huppert, Kerr & Sparks 1984). Much work on the quantitative physical chemistry of supersaturated solutions is still needed. Beyond A, crystals form, as evidenced by the momentary increase of temperature due to effects of latent heat. The density of the residual liquid of the lower layer, however, falls monotonically until it reaches that of the upper layer, after which overturning takes place.

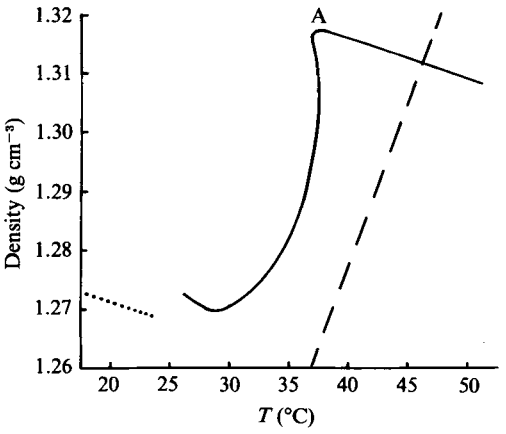

FIGURE 9. The solid curve is the measured density of a lower layer of aqueous KNO_3 as a function of its temperature. The dashed line is the density of saturated aqueous KNO_3 as a function of temperature. The dotted curve is the density of the upper layer as a function of its temperature.

Note that if the fluids of the two layers at their initial temperatures were mixed mechanically, the result would be a fluid mixture of the appropriately weighted mean temperature. No crystallization would occur, because the total volume would be undersaturated in both salts. The introduction of the lower layer, which remains distinct at the base of the container, allows it to evolve separately from the upper layer and crystallize in the smaller volume.

Geological significance

The ideas outlined by this simple experimental situation have important geological applications. Just as there are occasional eruptions from a magma chamber through the overlying volcano, so it is envisaged that there are occasional replenishments of the chamber with new, hotter, compositionally different and denser magma that originates from a greater depth within the Earth. This could occur by the injection of magmons. The new magma usually takes up a small fraction (maybe up to 1 or 2 %) of the total volume of the chamber. The space for it is made either by expansion of the chamber, due to the compression of the surrounding rock and magma, which can accommodate a volume increase of up to about 1 %, or by the surrounding rock cracking and being forced apart by injections of new magma into what are known as dykes or sills. These cracks may reach the surface and feed eruptions.

By far the most common magma chambers are those filled with basalt magma, at depths of a few kilometres beneath mid-ocean ridges. The input to these chambers is believed, from phase relations, laboratory simulation and theoretical evidence, to be of relatively high temperature ($\approx$ 1400 °C) and rich in magnesium oxide ($\approx$ 18 %). However, lavas with this chemical composition are rarely erupted. The question that vexed geologists for a number of decades was how to account for the difference between the predicted high MgO input and an output with much lower MgO content and temperature. The above model shows how fluid-mechanical principles can supply the answer.

A typical density against temperature relationship for a crystallizing, MgO-rich basalt is shown in figure 10, which also shows how temperature and composition are inter-related. Like the curve for saturated aqueous KNO_3 (figure 6), the density of the liquid basalt decreases from the point I as the temperature decreases. At the same time the amount of MgO in the magma decreases as it is taken up in the crystals that

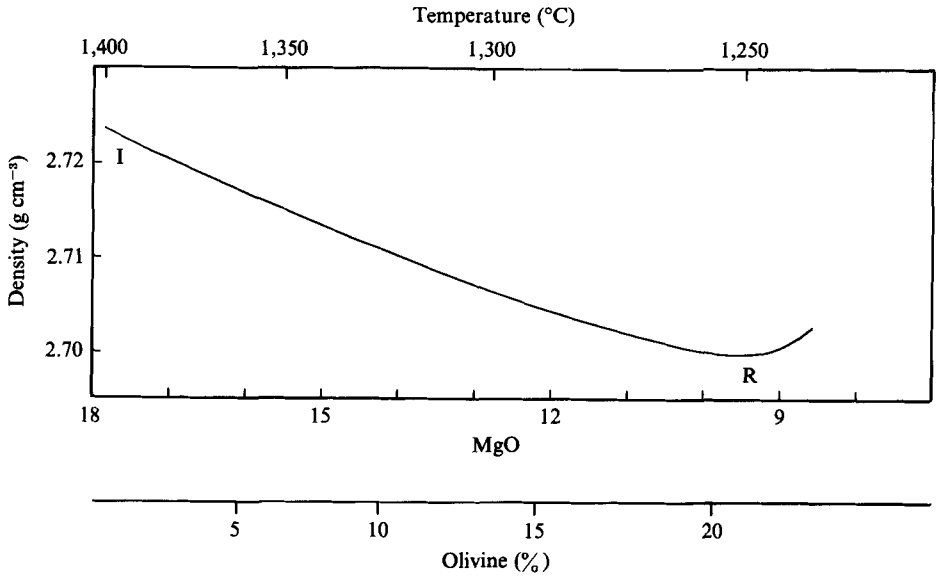

FIGURE 10. The density of fluid basalt magma as a function of either its temperature, its MgO content or the amount of olivine it has crystallized.

form, which are primarily Mg_2SiO_4 (olivine), the most abundant mineral in the Earth's mantle. This decrease in density continues until an MgO content of approximately 10% is reached (point R) beyond which the magma crystallizes a different mineral (plagioclase). The density of the residual liquid now begins to increase with decreasing temperature.

The question is then: what happens if magma of composition I is rapidly input into a chamber containing homogeneous magma of composition R?

The sequence of events that the model predicts is depicted in figure 11, where, for simplicity, the chamber is represented as having a rectangular cross-section. The input magma spreads along the bottom of the chamber as a dense gravity current (figure 11*a*). If the input momentum is large, the input may rise in the form of a fountain and mix somewhat with the resident magma before falling back to the bottom (Campbell & Turner 1985, 1986). In the Earth, where magma is driven by the buoyancy difference between it and the surrounding rocks, the vent must be very wide for any significant fountaining to take place. We shall not consider fountaining further here, but note that its main influence would merely be to bring the lower layer down the curve somewhat from its initial position I.

Once emplaced, the lower layer cools and begins to crystallize olivine, which reduces both the MgO content and the density of the liquid in the lower layer. In most magma chambers, the Rayleigh number of the lower layer typically exceeds 10^9. Hence, just as in the experiments, the motion is turbulent, and the initial root-mean-square turbulent vertical velocities can be shown to exceed by two or three orders of magnitude the low-Reynolds-number, free-fall speed of the small olivine crystals, whose dimensions are typically of the order of millimetres (Huppert & Sparks 1980*a*,*b*). Thus the olivine crystals remain in suspension and are carried around with the turbulent flow (figure 11*b*). Because the molecular diffusivity of MgO is much less than that of heat, virtually no material transfer accompanies the thermal transfer across the interface between the two layers. With time, the temperature

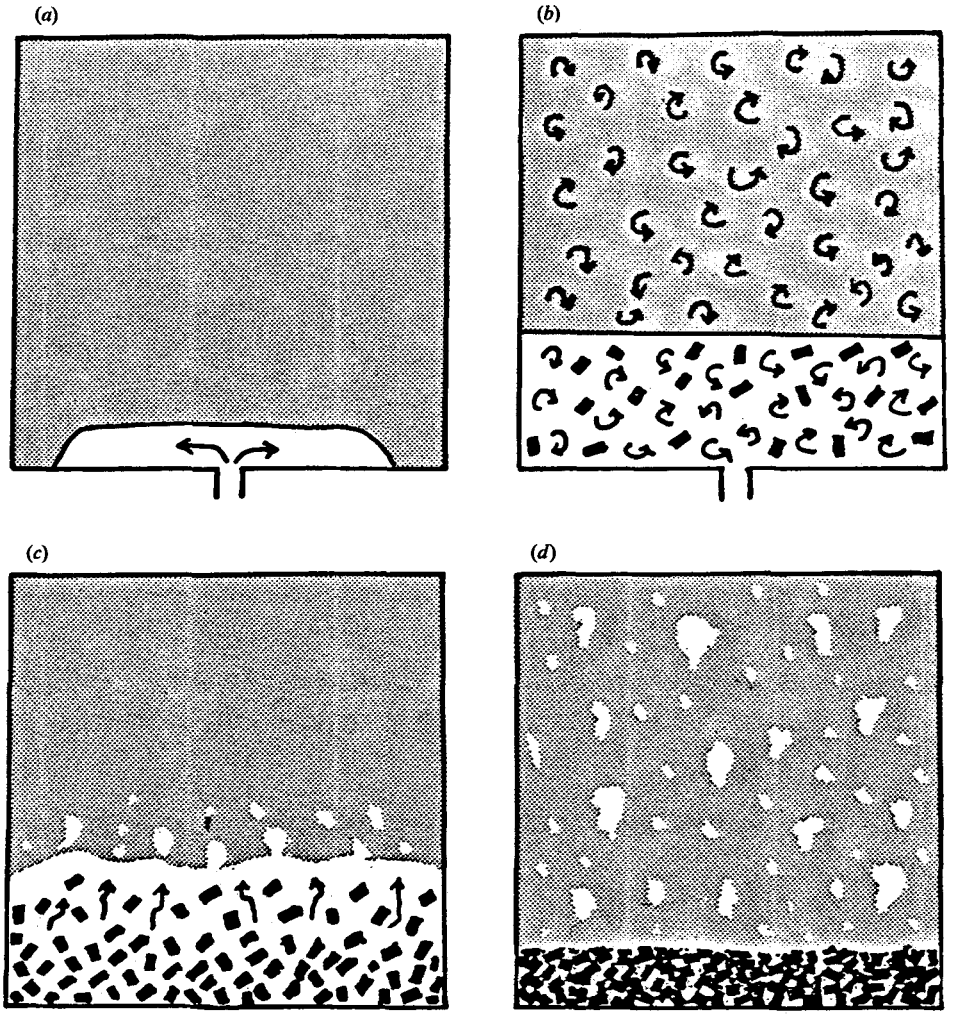

FIGURE 11. A cartoon representing the evolution of a magma chamber after the injection of new magma at its base. (*a*) Hot, heavy magma spreads along the base as a gravity current. (*b*) The separate lower layer cools and crystallizes, which induces vigorous convection in both layers. (*c*) The density of the residual liquid in the lower layer approaches that of the upper layer and the two layers mix (cf. figure 7) leaving the crystals at the base. (*d*) A dense mat of crystals remains behind.

difference between the two layers diminishes, as does the turbulent intensity. After a time, typically a few months, the olivines can no longer be held in suspension. They slowly sink to the bottom (figure 11*c*) and release magma whose MgO composition is much less than it was at input owing to the olivine formation. Cooling and olivine growth may continue until the density decreases sufficiently for the lower layer to rise and mix with the upper layer (figure 11*d*) to form one homogeneous layer. Further cooling and crystallization produces plagioclase, rather than olivine. The system may now be replenished again and the process will be repeated.

It is now believed that this is the explanation of prominent rock layers observed in the frozen remains of many magma chambers. An example of layering formed in this way is evident at Hallival on the Island of Rhum off north-west Scotland, as

shown in figure 12 (Plate 1). Sixty million years ago, Hallival was an active magma chamber, beneath an active volcano, which has since been eroded. Some fifteen layered units with thicknesses between 10 and 100 m have been carefully mapped (Brown 1956). Each unit consists of a thick, olivine-rich layer above which there is a very much thinner, plagioclase-rich rock layer (figure 12). All this is in agreement with the model. Detailed geochemical studies further substantiate the appropriateness of the model (Tait 1985).

The model has also been successfully applied to explain features seen in similarly layered rock in the Oman (as described in the volume edited by Coleman & Hopson 1981), in Montana, USA (Raedeke & McCallum 1984) and elsewhere.

Extensions

The above theory and associated laboratory experiment act as the basis for a number of extensions. They are all described in detail in the references listed below and make up the main material of the reviews by Huppert & Sparks (1984) and Sparks, Huppert & Turner (1984).

The first extension considers the influence of a continuous density gradient in the upper resident fluid (Huppert, Turner & Sparks 1982*c*). The evolution of the lower layer is as before until it begins to overturn, at which time its rise is constrained by the decreasing ambient density gradient.

Alternatively, if the input of hot, dense fluid is sufficiently slow, crystallization can take place almost immediately, because of the relatively large body of cold fluid into which the flow takes place (Huppert *et al.* 1982*c*). Experiments indicate that a significant fraction of the initial input fluid crystallizes, though in this case also released liquid with a decreased concentration rises into the resident fluid.

The basalt magmas that are injected into magma chambers filled with rhyolite or andesite, above the descending slabs at island arcs (on the rim of the Pacific and elsewhere), contain small quantities of dissolved water (≈ 1 or 2 wt %). Despite the differences in density and viscosity between input and resident magmas, the pumice erupted from the overlying volcanoes indicate that frequently the two magmas mixed quite intimately before eruption (figure 13, Plate 1). The vesiculated nature of the pumice suggests that before it solidified, the magma was rich in volatiles, and this provides an indication of how the mixing took place.

Huppert *et al.* (1982*b*) argued that the new, heavy magma ponds at the base of the chamber and then cools and crystallizes, as discussed above. The crystals that form are anhydrous and thus, as the temperature of the lower layer decreases, the relative concentration of the dissolved water in the melt increases. A point may be reached where the water becomes saturated. Thereafter the water will be exsolved as minute bubbles of water vapour. The gas, at the lower pressures of typical high-level magma chambers, is very much lighter than the melt and so the bulk density of saturated melt, crystals and bubbles can decrease dramatically. The bulk density of the lower layer may then decrease to that of the upper layer and the two layers will overturn. Saturated, relatively warm melt is then brought into contact with colder melt which releases more water vapour. This further increases the vigour of mixing between the two magmas. In a chamber of fixed volume, the pressure rises until it exceeds the tensile strength of the surrounding rocks. The magma chamber may then vent directly into the atmosphere.

Finally, it is interesting to examine the geological effects of different viscosities in the two layers. For example, experiments in which the upper layer was pure glycerine, with viscosity approximately 3000 times that of the hot aqueous lower layer, are

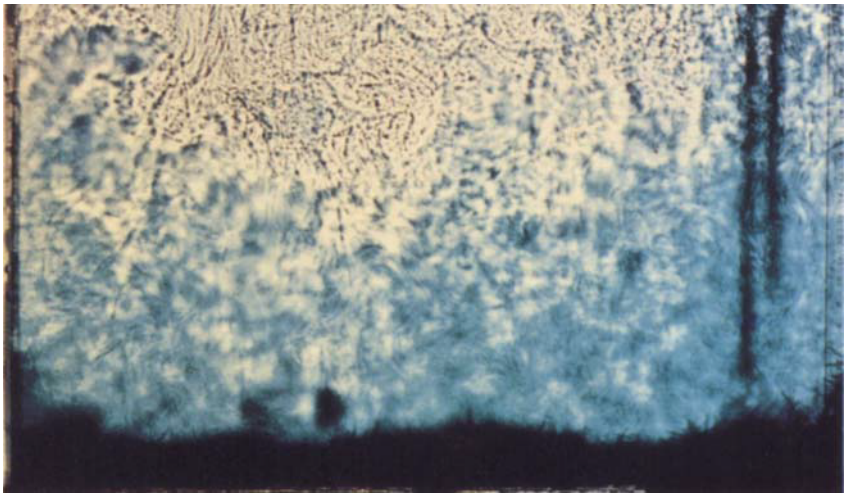

FIGURE 7. The residual liquid of an initially heavy layer of aqueous KNO_3 has just reached the same density as the fluid above and is mixing with it.

FIGURE 12. Hallival, on Rhum, a completely solidified magma chamber, incorporates layering induced by processes described in the text and sketched in figure 11. Photograph by C. H. Donaldson.

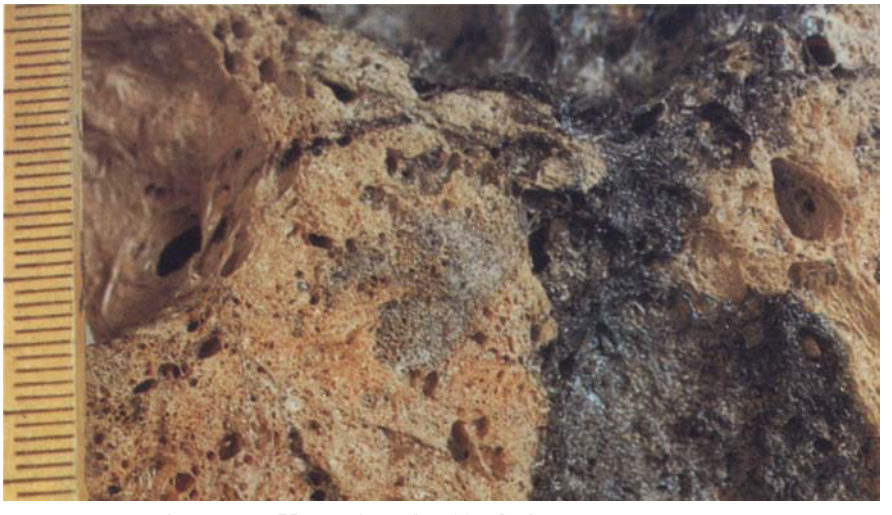

FIGURE 13. Pumice from the 1875 eruption of Askja, Iceland. A vein of basalt is mixed in with surrounding rhyolite, which also incorporates a blob of andesite.

(Facing p. 568)

FIGURE 14. A hot aqueous KNO_3 layer below glycerine. On crystallization, residual fluid rises as plumes or blobs undergoing further crystallization. Depleted aqueous KNO_3 migrates to the top.

FIGURE 17. Lava dome in the crater lake of the Soufrière of St. Vincent in 1972.

FIGURE 30. Cooling aqueous Na_2CO_3 at a central rod for 22 h. Photograph by J. S. Turner.

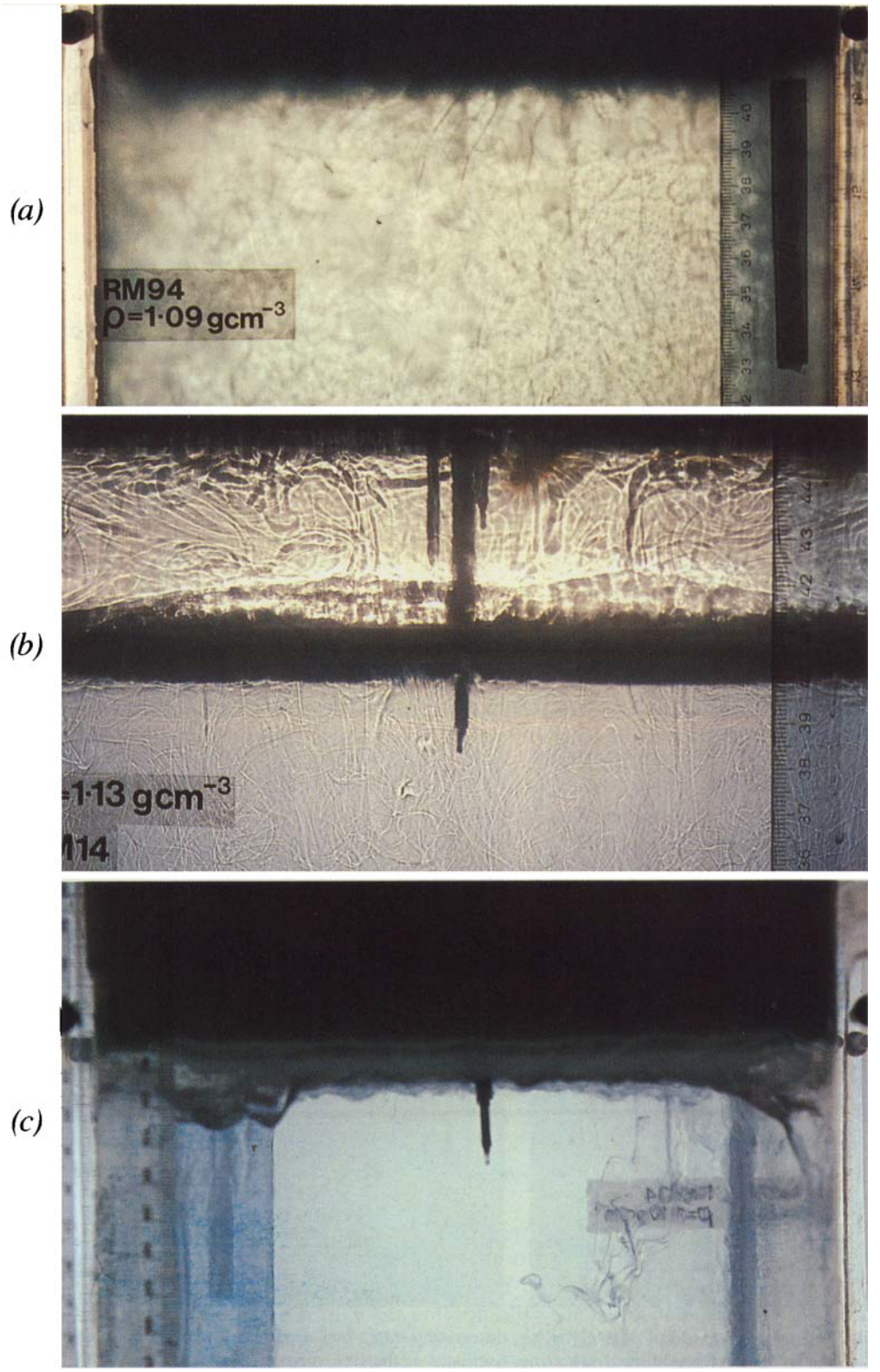

FIGURE 32. Melting a wax roof by hot fluid. Melt density *(a)* greater than, or *(b)* less than fluid density; and *(c)* either greater or less than fluid density, depending on temperature.

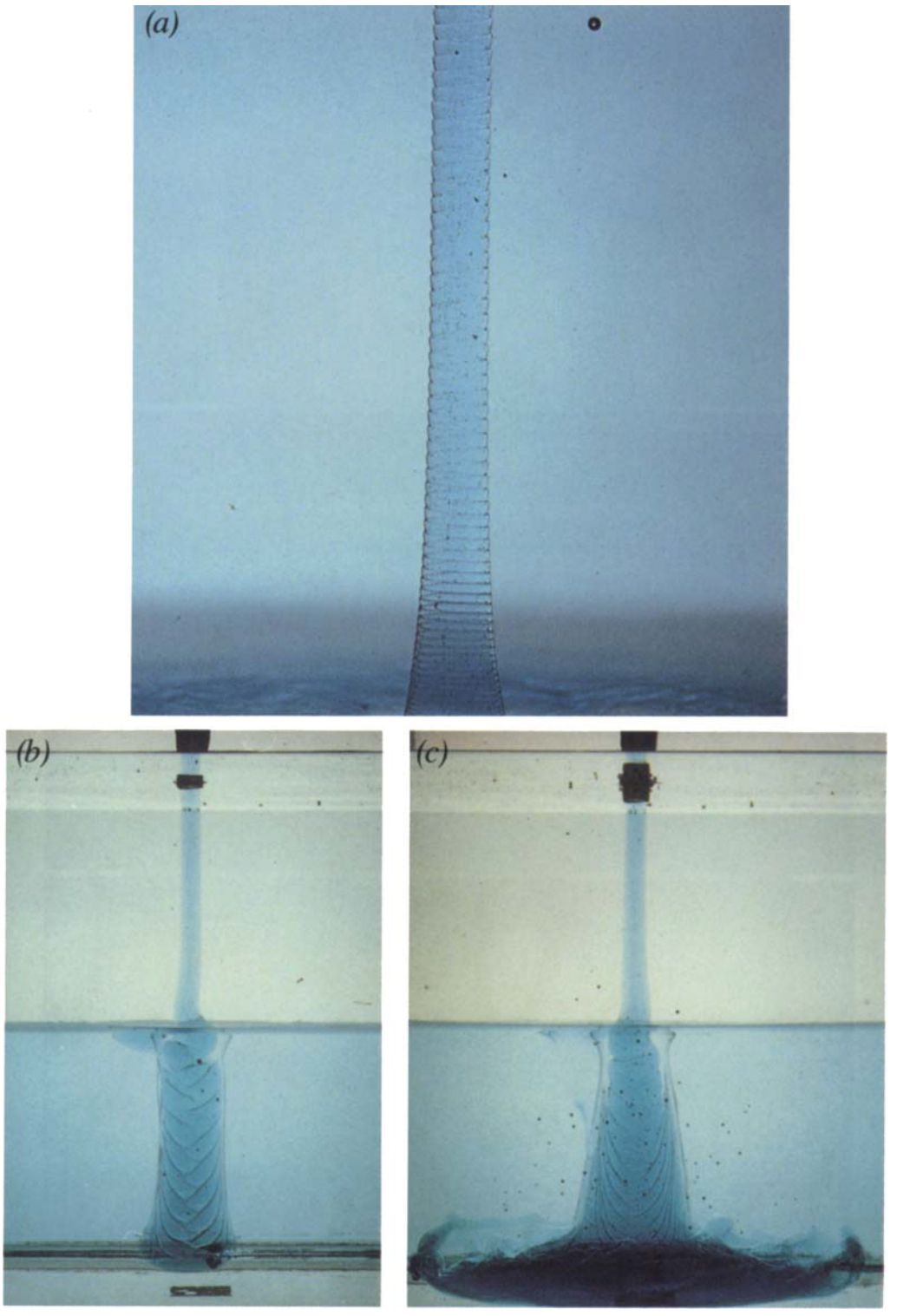

FIGURE 35. *(a)* A thin thread of pure glycerine, descending into a less dense layer of water and glycerine above a heavier layer of less diluted glycerine, oscillates at the free surface (just above the photograph) and the oscillations are carried down with remarkable regularity into the upper layer. *(b)* and *(c)* The source point of the glycerine in *(a)* is lowered below the free surface. The instability at the interface is taken down into the lower layer.

described by Huppert, Sparks & Turner (1983) and a much more extensive discussion is provided by Huppert, Sparks & Turner (1984). The new phenomenon displayed is that for sufficiently large viscosity contrasts, crystallization in the lower layer releases fluid which migrates almost immediately and continuously across the interface between the layers. The fluid rises in the form of buoyant plumes in which further crystallization takes place. Some crystals are sufficiently small that they are carried up by the vertical motion, while others fall out (figure 14, Plate 2).

4. Viscous gravity currents

Brief background

The spreading of viscous fluid across a horizontal surface occurs in many natural situations. The size of the fluid drop varies from the familiar cases of either liquid detergent spreading on a plate or honey on hard toast, through to volcanic lava flows. The latter often form axisymmetric domes, the radius and height of which can be of order 10^3 and 10^2 m respectively. For the first few months of their existence, the domes are covered by a blocky crust only a few tens of centimetres thick. During this time the lava in the dome cools surprisingly slowly through the crust because of the relatively large amount of latent heat released upon solidification. This keeps almost all the lava in the dome at an effectively uniform temperature and viscosity and allows the propagation of domes to be simulated by the spreading of viscous fluid on a plane. Accordingly, we now present a theoretical model for the spreading of an axisymmetric gravity current at low Reynolds number and determine the shape and rate of spreading of the resulting drop. A laboratory test of the theoretical results will then be presented using silicone oil as the experimental fluid. It will be shown how these results were used to determine the kinematic viscosity of the andesite lava dome formed by the eruption of the Soufrière of St Vincent in 1979. We conclude the section with an evaluation of the influences of a sloping surface on the flow.

Axisymmetric flow

Consider viscous fluid, density ρ, to be extruded at a point onto a rigid horizontal surface so that the volume extruded increases with time as Qt^α, as depicted in figure 15. It can be shown (Huppert 1982*a*) that viscous effects dominate inertial effects if $t \gg t_1 = (Q/g\nu)^{\frac{1}{2}(3-\alpha)}$ for $\alpha < 3$ or if $t \ll t_1$ for $\alpha > 3$. In these ranges, on the assumption that the radius of the current greatly exceeds its thickness, lubrication theory and the boundary conditions of zero velocity at the base of the current and zero stress at the unknown free surface $h(r,t)$ can be used to evaluate the velocity profile of the current as

$$u(r,z,t) = -\frac{g}{2\nu}h_r z(2h-z), \tag{4.1}$$

where surface tension has been neglected. This is permissible if the Bond number $B = \rho g l^2/\sigma \gg 1$, where l is the radius of the current and σ the surface tension. The expression (4.1) cannot be correct at the front of the current, but, as we shall see, this is immaterial. Expressed somewhat colloquially, the front does as it is told, and moves under a balance between pressure forces owing to the variation in height of the free surface and viscous forces in the main body of the current. The negligible influence on the motion of the front of the flow has important geological consequences, as we outline below.

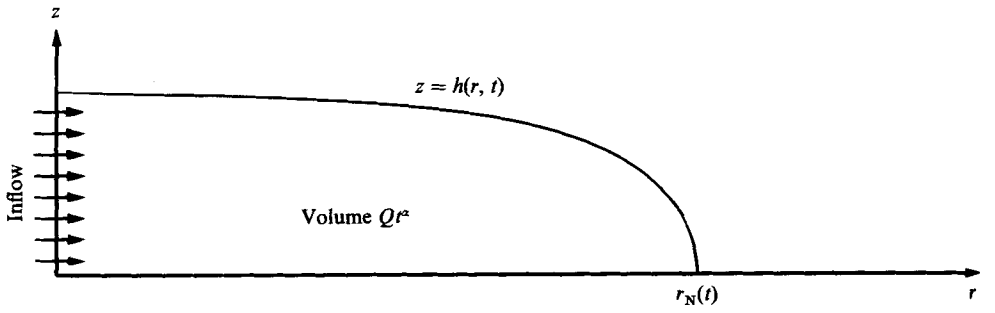

FIGURE 15. A sketch of a gravity current spreading across a horizontal plane.

A further relationship is obtained from the depth-integrated continuity equation

$$h_t + r^{-1}\partial_r\left(r\int_0^h u\,\mathrm{d}z\right) = 0. \tag{4.2}$$

Substituting (4.1) into (4.2), we obtain

$$h_r - \frac{g}{3\nu}r^{-1}\partial_r(rh^3h_r) = 0. \tag{4.3}$$

In order to solve (4.3) we need the global continuity equation

$$2\pi\int_0^{r_N(t)} rh(r,t)\,\mathrm{d}r = Qt^\alpha, \tag{4.4}$$

where $r_N(t)$ is the radius of the front, or nose, of the current.

The similarity solution of (4.3) and (4.4), to which all initial solutions must tend, can be expressed in terms of

$$\xi = \left(\frac{gQ^3}{3\nu}\right)^{-\frac{1}{8}} rt^{-\frac{1}{8}(3\alpha+1)} \tag{4.5}$$

and

$$h(r,t) = \xi_N^{\frac{3}{3}}\left(\frac{3\nu Q}{g}\right)^{\frac{1}{4}} t^{\frac{1}{4}(\alpha-1)}\psi(\xi/\xi_N), \tag{4.6}$$

where ξ_N is the value of ξ at $r = r_N(t)$. From (4.5), without further calculation, we can write the radius of the current as

$$r_N(t) = \xi_N\left(\frac{g'Q^3}{3\nu}\right)^{\frac{1}{8}} t^{\frac{1}{8}(3\alpha+1)}, \tag{4.7}$$

though ξ_N can only be obtained from the actual solution of the governing equations. This is done by substituting (4.5) and (4.6) into (4.3) and (4.4) to find that $\psi(y)$, where $y = \xi/\xi_N$, satisfies

$$(y\psi^3\psi')' + \tfrac{1}{8}(3\alpha+1)y^2\psi' - \tfrac{1}{4}(\alpha-1)y\psi = 0, \tag{4.8}$$

with

$$\xi_N = \left[2\pi\int_0^1 y\psi(y)\,\mathrm{d}y\right]^{-\frac{3}{8}}. \tag{4.9}$$

Together with the boundary condition $\psi(1) = 0$, (4.8) represents a well-posed problem. Numerical solutions for various α are given in Huppert (1982*a*).

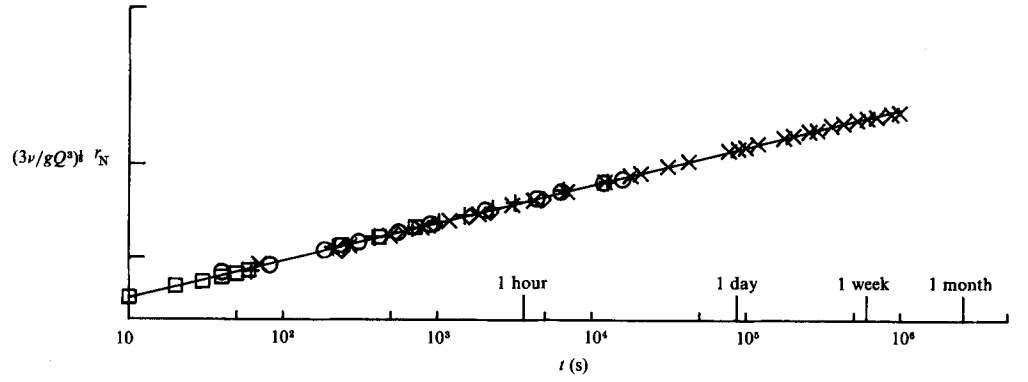

FIGURE 16. The non-dimensionalized radius of five gravity currents in the laboratory as functions of time compared with the theoretical prediction (4.7).

Experimental confirmation

Because of the neglect (some critics said disregard) of conditions at the front of the current, such as surface tension and contact-line effects, it seemed imperative to test experimentally the spreading relationship (4.7). Accordingly, the spreading of two silicone oils, of viscosities 13.2 and 1110 $cm^2\ s^{-1}$, on a horizontal Perspex sheet was monitored. Five experiments with $\alpha = 0$ were carried out using different initial conditions, such as pouring the oil onto the Perspex, releasing it from either a right circular cylinder or from a parabolic-shaped cylinder. The method of initiation made no difference to the flow after the first few seconds of the release. Figure 16 presents for all five experiments the measured radius as a function of time, non-dimensionalized in the way suggested by (4.7). Also plotted in the figure is the theoretical relationship (4.7). The agreement between theory and experiment was rather encouraging.

Additional data on the height of the current at the centre and from experiments with constant flux release were all in good agreement with the theory. Further details are given in Huppert (1982*a*) and Huppert *et al.* (1982*a*). The general conclusion is that, despite the neglect of all effects at the front of the current, the theory is capable of describing accurately the motion in a real situation.

The 1979 eruption of the Soufrière of St. Vincent

The Soufrière of St. Vincent in the West Indies is a 1200 m high volcano which has erupted at intervals over at least the last 300 years, and probably over the last 4000 years. The volcano has a summit crater 1.6 km in diameter and some 300 m deep. The first eruption this century was in 1902 when 2 km^3 of solid rock was ejected and 1500 people were killed. After 1902 the crater was partially filled with rainwater and a lake with a depth of order 100 m formed. During 1971/2 a lava dome was slowly and quietly extruded into the lake with no accompanying seismic activity but with the release of a considerable smell of sulphur. Unfortunately, most of the dome was underwater and so systematic observations of the shape, volume or radius as functions of time were impossible. Figure 17 (Plate 2) presents a photograph of the dome in its later stages.

On 13 April 1979 the volcano erupted explosively. It continued erupting until 26 April by which time the 1971/2 extrusion had been destroyed and the crater lake

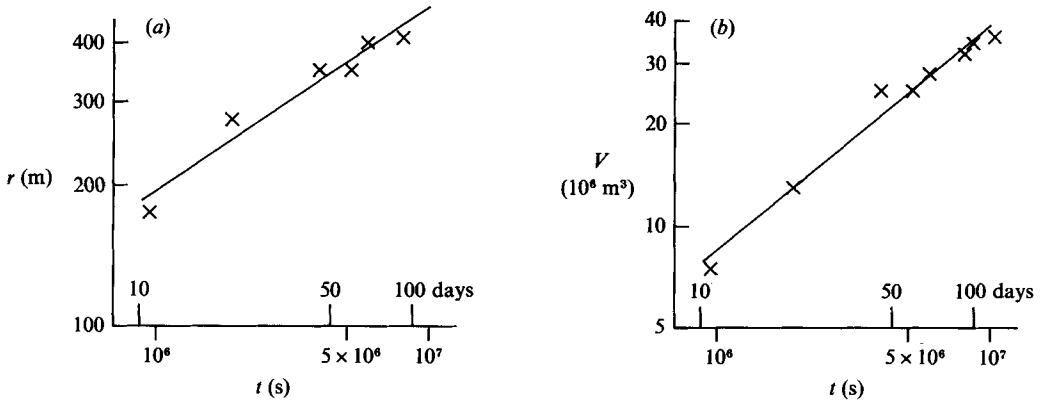

FIGURE 18. (a) The measured radius, and (b) the evaluated volume of the 1979 dome of the Soufrière of St. Vincent and the lines of best fit to the data.

no longer existed.† The crater floor reverted to the dry, relatively flat base that existed prior to 1902. Starting late in April and continuing through to the end of September, a lava dome of andesite was slowly extruded over the crater floor. Before the beginning of October, the volume of the dome had arrived at its final value. Motion in the dome had effectively ceased and part of the dome had spread up to the crater wall. By that time the mean diameter of the dome was 870 m, the highest point above the crater floor 130 m and the estimated amount of lava discharged was 50×10^6 m^3.

During the first five months of existence of the lava dome, its radius and height were carefully observed on sixteen separate occasions by Aspinall, Rowley, Shepherd, Sigurdsson & Tomblin (Huppert *et al.* 1982*a* and references therein). From the measurements taken it is possible to estimate fairly accurately the volume of the dome at these times. Figure 18 presents the volume V and radius r of the dome as a function of time on a log–log scale.‡ Also graphed on figure 18 are the best-fit straight lines to the first 8 data points, taken while the dome was growing. These can be written (in m.k.s. units) as

$$r = 90t^{0.39}, \quad V = 933t^{0.66}. \tag{4.10a,b}$$

Consider the assumption that the spreading of lava domes can be analysed by a constant-viscosity model. At first sight it may seem rather surprising that such an assumption can lead to meaningful results. That it can is validated by the arguments briefly described at the beginning of the section and presented in greater detail in Huppert *et al.* (1982*a*). With this procedure the observed relationships (4.10) can be used with the theoretical relationship (4.7) to obtain results of considerable geological interest. When comparing the laboratory results with the theoretical relationship, we knew g, Q, ν and α and compared the values of $r_N(t)$ measured in the laboratory with the theoretically predicted values. In the geological situation we know $g, r_N(t)$ from (4.10*a*) and $Q = 933$ and $\alpha = 0.66$ from (4.10*b*). Two calculations can then be carried out. First, we can use the value of α determined from (4.10*b*) to confirm that the

† A visit to the crater at the end of April by representatives of the Dangerous Sports Club of Oxford is imaginatively described by Cranfield (1983).

‡ The data set plotted here is that originally drawn up by Tomblin (Westercamp & Tomblin 1979). The data discussed in Huppert *et al.* (1982*a*) are sightly different; however, the conclusions reached are the same for either data set.

measured power-law relationship (4.10*a*) is consistent with the theory, which predicts a power of $\frac{1}{8}(3\alpha+1) = 0.37$. The comparison of this value with 0.39 is as satisfactory as one could hope for. Secondly, one can determine the coefficient of viscosity from the measured coefficient in (4.10*a*). This leads to a value of 6×10^{11} cm^2 s^{-1}, which is roughly consistent with what might have been expected knowing the composition of the lava and its extrusion temperature. It should be borne in mind, however, that obtaining *in situ* measurements of the viscosity of lava are fraught with difficulty. Moreover, theoretically determined values dependent on composition and temperature are heavily based on empirical relationships. Since viscosity varies so greatly with both temperature and composition, the usual *in situ* methods of determining viscosity can be quite inaccurate. The stimulating possibility of the approach outlined above is that it can yield results easily and quite accurately.

Extensions

A number of extensions immediately suggest themselves, some of which will be briefly discussed. First, the gravity current could propagate into a deep fluid of density $\rho-\delta\rho$ whose viscosity is comparable with that of the intruding current. Then the motion in the upper fluid is due entirely to viscous diffusion driven by the motion of the current itself. Across the top surface of the current the shear stress is continuous. However, order-of-magnitude estimates of the shear stress at the base of the intruded fluid (Huppert 1982*a*) show it to be negligible and hence the condition of zero shear stress at the top of the current is obtained to a good degree of approximation in this case also. The only difference is that, as usual, $g' = g\delta\rho/\rho$, replaces g in the expressions (4.1), (4.3) and (4.5)–(4.7).

The second extension is to a two-dimensional current, rather than an axisymmetric geometry. The ideas outlined above carry over, and one can easily show that the length of the current $x_N(t)$ satisfies

$$x_N(t) = \eta_N\left(\frac{g'q^3}{3\nu}\right)^{\frac{1}{5}} t^{\frac{1}{5}(3\alpha+1)}, \tag{4.11}$$

where the area of the current is given by qt^α and η_N is graphed in Huppert (1982*a*).

It is then natural to investigate the effects of two confining walls parallel to the flow direction. In general this leads to a rather complicated governing equation. A somewhat surprising result, however, can be readily obtained in the limit in which the spacing between the walls L is very much less than the typical height of the current. In this limit the governing equation for the free-surface height $h(x,t)$ is

$$h_t - \frac{gL^2}{12\nu}(hh_x)_x = 0 \tag{4.12}$$

and

$$\int_0^{x_N(t)} h(x,t)\,\mathrm{d}x = qt^\alpha. \tag{4.13}$$

The similarity solution to (4.12) and (4.13) is given by

$$h(x,t) = \chi_N^2\left(\frac{12q^2\nu}{gL^2}\right)^{\frac{1}{3}} t^{\frac{1}{3}(2\alpha-1)}\,\phi\left(\frac{\chi}{\chi_N}\right) \tag{4.14}$$

and

$$\chi = \left(\frac{gL^2q}{12\nu}\right)^{-\frac{1}{3}} x t^{-\frac{1}{3}(\alpha+1)}, \tag{4.15}$$

where $\phi(w)$ satisfies

$$(\phi\phi')' + \tfrac{1}{3}(\alpha+1)\,w\phi' - \tfrac{1}{3}(2\alpha-1)\,\phi = 0. \tag{4.16}$$

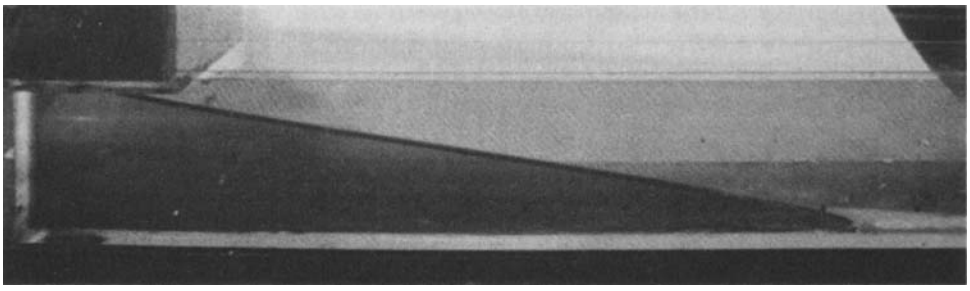

FIGURE 19. A gravity current propagating between two closely spaced walls. Note the form of the front of the current, which is in agreement with the theoretical prediction. Experiment and photography by T. Maxworthy.

The solution of (4.16) around $w = 1$ can be expressed in terms of the regular power series

$$\phi = \tfrac{1}{3}(\alpha+1)(1-w)+\tfrac{1}{12}(\alpha-2)(1-w)^2+O(1-w)^3, \tag{4.17}$$

which indicates that for all α the free surface at the nose of the current intersects the base at a finite slope (and not at the 90° appropriate for axisymmetric or two-dimensional currents). This prediction was verified by T. Maxworthy (private communcation), who kindly supplied the experimental photograph reproduced in figure 19.

Flows down slopes

The foregoing has considered spreading on a horizontal surface, in which case the driving force is the pressure gradient due to the slope of the free surface. If, on the other hand, the flow is down an inclined plane, the down-slope gravitatonal force is more important. Consider a flow, initiated, say, by releasing a gate so that at the release there is no variation in the direction along the slope, which is at constant angle θ. The first question to discuss is whether a two-dimensional flow (uniform in the cross-slope direction) will result. On the assumption, as before, that the Bond number is small and that the concepts of lubrication theory are appropriate, the governing equations can be solved fairly directly. Some time after the initiation of the flow, no matter what the initial shape, the free-surface profile takes the form (Huppert 1982*b*)

$$h(x,t) = \left(\frac{\nu}{g\sin\theta}\right)^{\frac{1}{2}} x^{\frac{1}{2}}t^{-\frac{1}{2}} \tag{4.18}$$

for

$$0 < x \leqslant x_{\mathrm{N}} = \left(\frac{9A^2 g\sin\theta}{4\nu}\right)^{\frac{1}{3}} t^{\frac{1}{3}}, \tag{4.19}$$

where x is the down-slope coordinate (with $x = 0$ at the back of the current and $x = x_{\mathrm{N}}$ at the front or nose) and A is the initial cross-sectional area. Note that the profile of the predicted current ends abruptly at $x = x_{\mathrm{N}}$ (indicating a total disregard for conditions at the front of the flow).

A series of experiments were undertaken to test the theoretical relationship (4.19). The same Perspex sheet used previously was held at an angle and fluid was poured into the space between a back edge and a removable gate 5 cm down-slope. Some thirty experiments were conducted with three different fluids. At first the motion was virtually independent of the cross-slope coordinate except near the walls where viscous drag retarded the flow. The observed length of the current as a function of time is plotted in figure 20 for a number of experimental runs. The experimental and theoretical results are in close agreement, which justifies the neglect of both

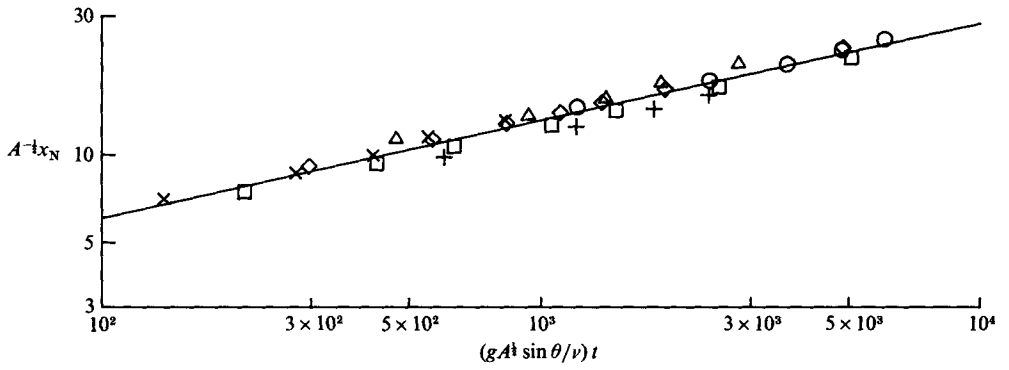

FIGURE 20. The length of a two-dimensional current down a slope, normalized with respect to $A^{\frac{1}{2}}$, as a function of a suitably non-dimensionalized time. The straight line is the theoretical prediction (4.19) and the experimental points are for six typical runs.

surface-tension and contact-line effects in predicting the temporal development of the two-dimensional current.

The two-dimensional flow continued for quite some time until, almost spontaneously, the flow front became unstable, and a series of small-amplitude waves of fairly constant wavelength across the slope began to grow. The wave amplitude increased with time as the maxima (points furthest down the slope) propagated faster than the minima. The wavelength remained unaltered. The long-time shape of the flow front depended on whether the fluid was silicone oil or glycerine. Flows with silicone oil developed the form shown in figure 21 (*a*): periodic, triangular fronts with tightly rounded maxima. These maxima were connected by very straight portions at an angle to the slope to extremely pointed minima. Flows with glycerine developed the form shown in figure 21 (*b*): periodic, less tightly rounded maxima, again connected by extremely straight portions, but in this case the boundaries were almost directly down-slope and connected to very broad minima. Silvi & Dussan V. (1985) performed experiments with glycerine flowing down a *glass* surface and found that the final form was very similar to that in figure 21 (*a*), i.e. to that displayed by silicone oil on a Perspex surface.

The cause of the instability is the effect of surface tension at the front of the current. In general, the solution of the instability of a free-surface flow that is dependent on both space and time is a formidable task. In this case, however, Huppert (1982*b*) was able to employ a scaling analysis, which suggests that the wavelength of the instability, $\lambda \propto (A^{\frac{1}{2}}\sigma/\rho g \sin\theta)^{\frac{1}{3}}$. This was confirmed by the experiments, which indicated further that the constant of proportionality is 7.5. It would be interesting to determine the solution of the subsequent flow field, with its straight boundaries, but this has not yet been accomplished. Even the importance of surface-tension and contact-line effects in this regime have not been ascertained.

Some further experiments have been undertaken using an aqueous polyacrilimide solution. A 1.5 wt % solution is extremely non-Newtonian with a coefficient of shear viscosity that varies from approximately 10^5 cm^2 s^{-1} at a shear of 1 s^{-1} to 10^{-1} cm^2 s^{-1} at a shear of 10^3 s^{-1}. In the two-dimensional regime, the flow progagated at a rate which was well predicted by altering the theoretical analysis to incorporate the non-Newtonian relationship between stress and rate of strain. On Perspex, the instability developed as before and took the shape depicted in figure 21 (*b*).

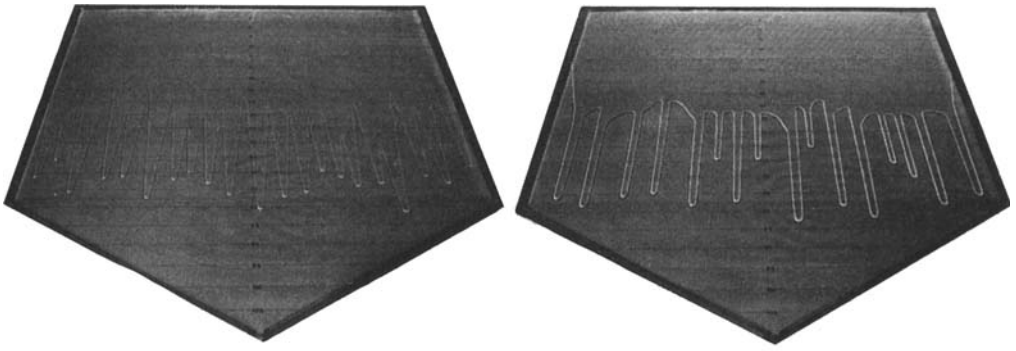

FIGURE 21. The two different froms of finite-amplitude motion of an initially two-dimensional viscous gravity current down a Perspex slope of 12°. (*a*) silicone oil 185 s after release; (*b*) glycerine 62 s after release.

5. Hot, turbulent flows over erodible beds

During the Archean age, between 4.0 and 2.5×10^9 years ago, some of the lavas erupted onto the surface of the Earth were hotter (*c.* 1600 °C) and much less viscous (*c.* 1 cm^2 s^{-1}) than lava erupted today. The lower viscosity was partly due to the higher temperature and partly due to the lower SiO_2 content of the depolymerized melt. The lavas are called komatiites after the Komati River in South Africa where their solid remnants were first identified in 1969. They have now also been reported in Australia, Brazil, Canada, Finland, the Soviet Union and Zimbabwe. The available evidence suggests that the komatiites were erupted from long fissures (maybe hundreds or even thousands of metres long) onto the floor of the Archean ocean. Calculations of the Reynolds number of the output indicate that for many of the eruptions the flow was turbulent for tens of kilometres from the source (Huppert *et al.* 1984 and Huppert & Sparks 1985). The suggestion put forward in these papers is that the turbulently flowing lavas were capable of melting the underlying rock, whose melting temperature would have been between 850 and 1200 °C depending on its composition. As a consequence of the melting process, the lava was contaminated by the ground over which it flowed, which the authors suggested could be used to explain the formation of most of the world's accessible supply of nickel.

This geological background motivates the study of a two-dimensional line source of hot fluid flowing turbulently below a large body of water and over initially solid ground.

Theoretical considerations

Consider fluid of density ρ and initial temperature T_0 issuing at a (two-dimensional) flow rate Q beneath another fluid of density $\rho - \delta\rho$ (with $\delta\rho > 0$) and initial temperature T_∞. If the Reynolds number of the flow remains greater than approximately 500, the resulting gravity current is turbulent, and the velocity of advance is independent of the Reynolds number (Simpson & Britter 1979). The thickness h can then be determined from

$$h = \left(\frac{Q^2}{2g'}\right)^{\frac{1}{3}}, \quad g' = \frac{g\delta\rho}{r} \tag{5.1a,b}$$

(Britter & Linden 1980). As a current of this thickness flows over the ground, it transfers heat to the ground and melts it.

To analyse this melting it is instructive to investigate first the thermal problem

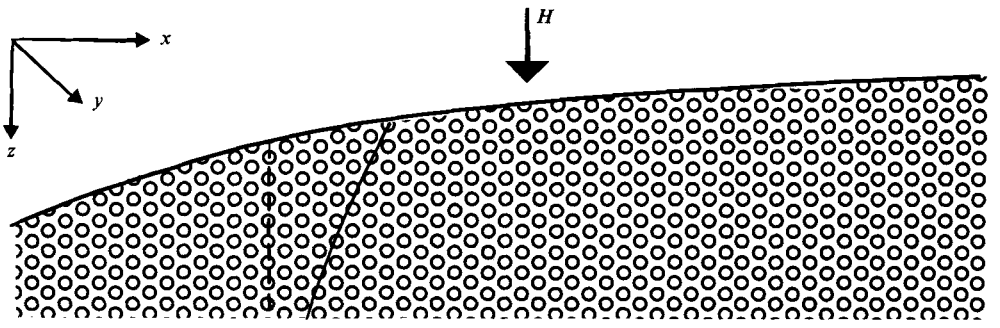

FIGURE 22. A sketch of a heat flux H applied to a solid surface which melts under its action.

sketched in figure 22. Consider a heat flux $H(x, y)$ applied at the surface $z = \eta(x, y, t)$ of a semi-infinite solid of density ρ†, specific heat c, thermal diffusivity κ and latent heat L, whose melting temperature is T_m. Within the solid, the temperature T satisfies

$$T_t = \kappa \nabla^2 T, \tag{5.2}$$

$$T[x, y, \eta(x, y, t)] = T_m, \tag{5.3}$$

$$T \to T_\infty \quad (z \to \infty). \tag{5.4}$$

Assuming that the horizontal scales l_x and l_y greatly exceed the vertical scale l_z, which we shall see is of order κ/η_t, the horizontal derivatives can be neglected in (5.2) and the solution written as‡

$$T = T_\infty + (T_m - T_\infty) \exp\left[-\eta_t \frac{(z-\eta)}{\kappa}\right]. \tag{5.5}$$

Conservation of heat at the interface $z = \eta$ requires

$$H = -\rho c \kappa T_z[x, y, \eta(x, y, t)] + \rho L \eta_t. \tag{5.6}$$

Substituting (5.5) into (5.6) and rearranging, we obtain

$$\eta_t = \frac{H}{\rho c (T_m - T_\infty + L c^{-1})}, \tag{5.7}$$

which indicates that η varies linearly with time. Equation (5.7) expresses the fact that the rate of melting η_t is a balance between the heat input H and the heat necessary to bring the solid up to its melting temperature, T_m, from T_∞ and then to melt it.

Returning now to the turbulent gravity current, it transfers heat to the underlying solid and also to the overlying fluid. Assuming that the temperature of the overlying fluid is less than the freezing temperature of the fluid that makes up the current, the heat loss at the top of the current causes a solid crust to form above it. How the heat is taken away from the top of the crust is immaterial to the present investigtion;

† Use of this symbol anticipates that, for simplicity, we shall equate the density of the gravity current to that of the ground over which it flows. Unequal densities are considered in Huppert *et al.* (1984) and Huppert & Sparks (1985).

‡ Only the steady-state solution is considered here. The investigation of the transient response to the initial-value problem raises some interesting questions, which I plan to discuss in a future publication. It will be shown that the timescale of the transient response is $\rho^2 c^2 (T_m - T_\infty)^2 \kappa / H^2$ and the resultant thickness of solid affected is $\rho c^2 \kappa (T_m - T_\infty)^2 / LH$. Both these values are entirely negligible in the geological context.

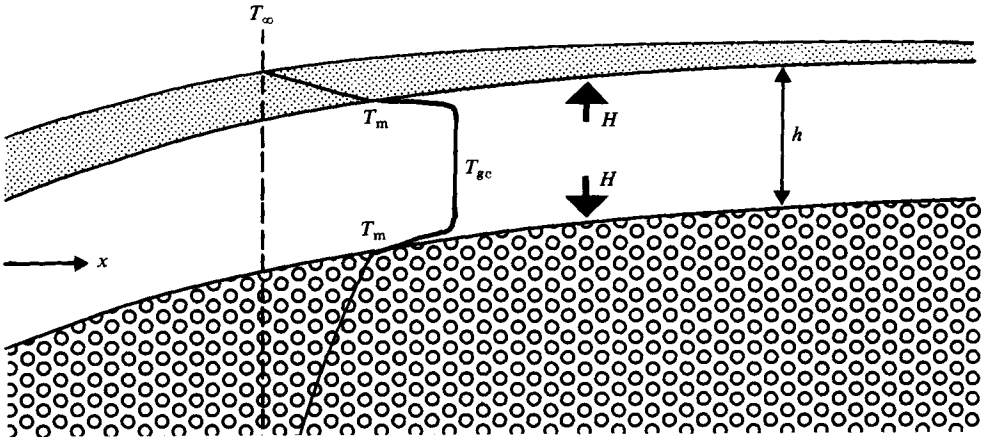

FIGURE 23. A sketch of a hot, turbulent gravity current propagating over an erodible bed and forming a thin crust at the top of the current.

convective or other motions in the upper fluid are generated as required and maintain a constant temperature. Suppose, for simplicity of exposition, that the freezing temperature of the fluid which makes up the gravity current is the same as the melting temperature of the ground. Then the heat transferred to the ground equals that transferred to the over-riding crust and each can be equated to H above. Denote the mean temperature in the gravity current by $T_{gc}(x)$ with respect to an x-axis in the direction of flow, as in the sketch of figure 23. A turbulent flow of mean temperature T_{gc} maintained at temperature T_m at its extremities transfers heat at top and bottom at a rate H, given by

$$H = h_T(T_{gc} - T_m), \tag{5.8}$$

where h_T is a heat transfer coefficient which is dependent upon the Prandtl number and Reynolds number of the flow (Holman 1976). Because of this dependence, h_T varies with x. However, in the geological context, the variation is small in the main part of the flow (Huppert *et al.* 1984) and we shall here neglect its effects.† A local heat balance for the gravity current then leads to

$$\rho c h \dot{T}_{gc} = 2h_T(T_{gc} - T_m) - \frac{h_T(T_{gc} - T_m)^2}{T_m - T_\infty + Lc^{-1}}. \tag{5.9}$$

where $\dot{T}_{gc}$ signifies the temporal derivative of T_{gc}. The first term on the right-hand side represents the heat lost from the current at the top and bottom of the flow, while the second represents the heat needed to raise the melt from its melting temperature to that of the gravity current. The temporal derivative can be converted to a spatial derivative by

$$\frac{\mathrm{d}}{\mathrm{d}t} = u\frac{\mathrm{d}}{\mathrm{d}x}, \tag{5.10}$$

where

$$u = \frac{Q}{h} = (2g'Q)^{\frac{1}{3}}. \tag{5.11a,b}$$

† This approximation is not made by Huppert & Sparks (1985), who arrive at a nonlinear differential equation with non-constant coefficients which they solve numerically. Our procedure will lead to a nonlinear differential equation that can be solved analytically and so permits a more penetrating interpretation. Unfortunately, however, the approximation dismisses the fact that after sufficient distance the Reynolds number of the flow will have decreased sufficiently that the flow is no longer turbulent, and $h_T \approx 0$.

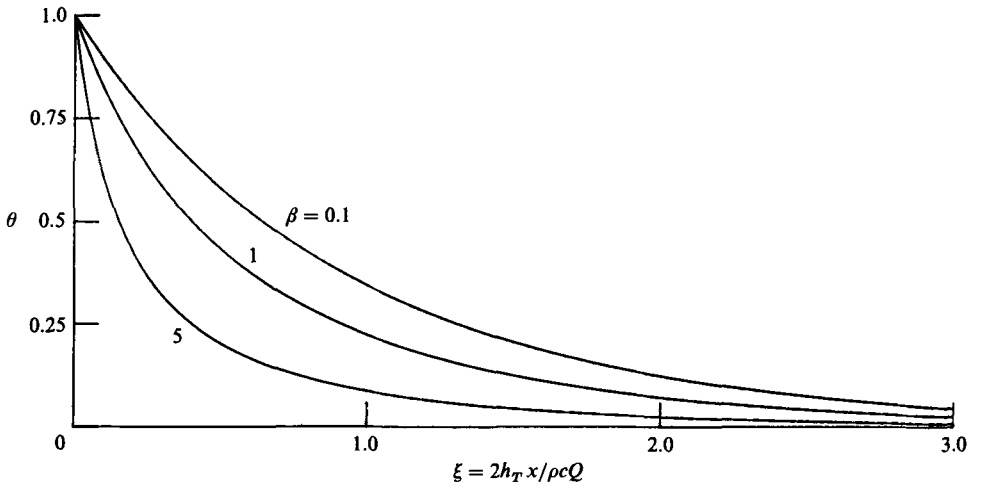

FIGURE 24. The non-dimensional temperature as a function of the non-dimensional distance for three values of β defined by (5.16) for a hot, turbulent gravity current propagating over an erodible bed.

Introducing the non-dimensional temperature θ by

$$\theta = \frac{T_{\rm gc} - T_{\rm m}}{\Delta}, \tag{5.12}$$

where

$$\Delta = T_{\rm gc}(x = 0) - T_{\rm m} \tag{5.13}$$

and the non-dimensional length in the flow direction by

$$\xi = x/l_x, \tag{5.14a}$$

where

$$l_x = \tfrac{1}{2}\rho c Q/h_T, \tag{5.14b}$$

into (5.9) and using (5.10), we can solve for the temperature as a function of downstream distance as

$$\theta = [(\beta+1)\,{\rm e}^{\xi} - \beta]^{-1}, \tag{5.15}$$

where

$$\beta = \frac{\frac{1}{2}\Delta}{T_{\rm m} - T_{\infty} + Lc^{-1}} \tag{5.16}$$

is independent of h_T. The quantity β is a ratio of the specific heat released as the input fluid is cooled to its freezing point to the specific heat needed to raise ground to its melting temperature plus the latent heat to melt it. Flows with large β could be considered thermally energetic; those with small β thermally weak. Solutions as functions of ξ for various β are graphed in figure 24.

The relative contamination C, which is the volume of melted ground added to the current per unit volume of initial material that makes up the current, is given by

$$C = Q^{-1} \int_0^x \eta_t \, {\rm d}x. \tag{5.17}$$

Substituting (5.7), (5.8) and (5.12) into (5.17) and using (5.14) and (5.15) to evaluate the integral, we obtain

$$C = \ln[(\beta+1)\exp(\xi) - \beta] - \xi \tag{5.18}$$

$$\to \ln(\beta+1) \quad (\xi \to \infty). \tag{5.19}$$

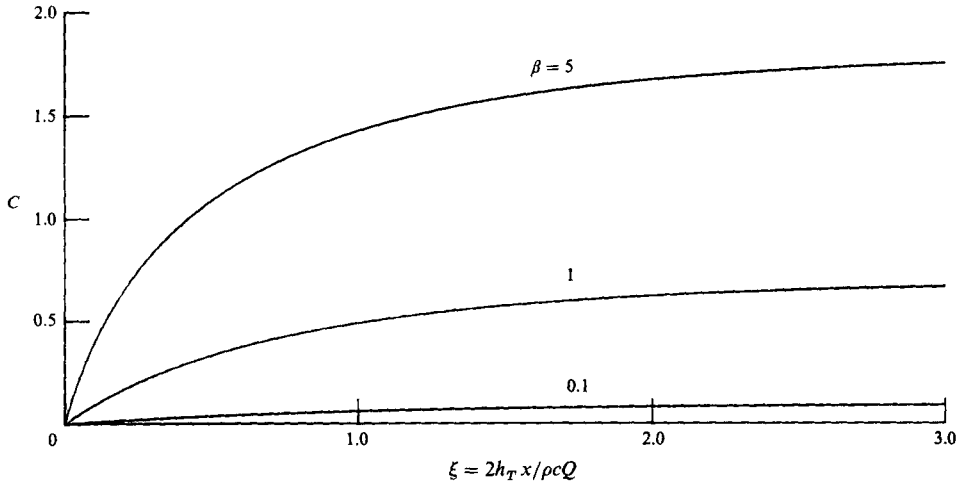

FIGURE 25. The relative contamination as a function of the non-dimensional distance for the same cases as in figure 24.

This shows that the contamination far downstream of the source approaches a finite value. Graphs of C as a function of ξ for various values of β are presented in figure 25. The crust that forms above the current adjusts rapidly to the equilibrium thickness which is determined from equating the heat input H to the conductive flux $\rho c\kappa(T_m - T_\infty)/a$, where a is the thickness of the crust, and the temperature of the water is assumed, for simplicity, to be T_∞. Using (5.8), (5.12) and (5.14) to evaluate H, we can determine a to be given by

$$a = \rho c\kappa h_T^{-1} \Delta^{-1}(T_m - T_\infty)\,[(\beta+1)\,e^{\xi} - \beta]. \tag{5.20}$$

This crustal thickness is a stable solution to the equations in the sense that were it to increase (due to some perturbation), the conductive flux could not carry away all the heat incident at the bottom of the crust, which consequently would melt. A decrease in thickness would extract heat from the top of the current and cause it to solidify. Mathematically, this is expressed by

$$\rho L\dot{a} = H - \frac{\rho c\kappa(T_m - T_\infty)}{a}. \tag{5.21}$$

While (5.21) does not have a solution in closed form, it does permit us to evaluate the timescale of the relaxation to the basic state (5.20) as

$$\rho^2 c\kappa L \Delta^{-2} h_T^{-2}(T_m - T_0)\,[(\beta+1)\,e^{\xi} - \beta]^2. \tag{5.22}$$

Experimental confirmation

We (Huppert & Sparks 1985) thought that it would be instructive to carry out a qualitative experimental test of the ideas of thermal erosion developed above. We allowed water at an initial temperature of about 65 °C to flow down a smooth, solid surface made of Polyethylene glycol 1000 (PEG 1000) which has a melting temperature between 37 and 40 °C and is completely miscible with water. The water issued from a horizontal spout 1.5 cm wide onto a 2° slope. Various experiments at different flow rates were conducted.

For the slowest flow rates, surface tension and contact-line effects at the edges of

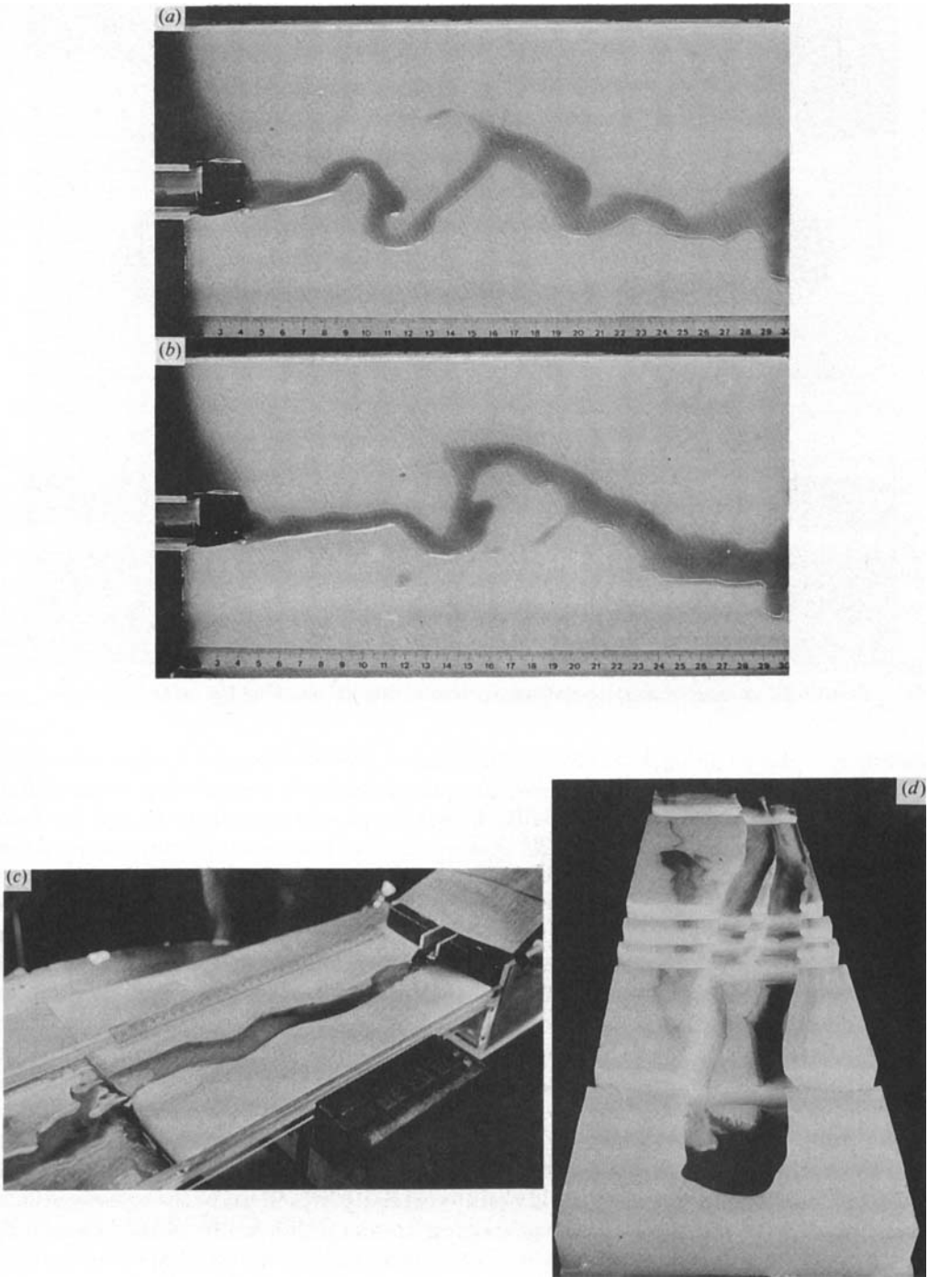

FIGURE 26. Photographs of hot, dyed water flowing down a wax slope. (*a*) and (*b*), taken after 8 s and 12 s respectively, with a rather slow flow rate, show the initial instability generated by contact-line and surface-tension effects before the formation of a thermal-erosion channel; (*c*) taken after 4.5 min shows a well-developed thermal erosion channel; (*d*) displays a downstream view, with a number of cross-cut sections.

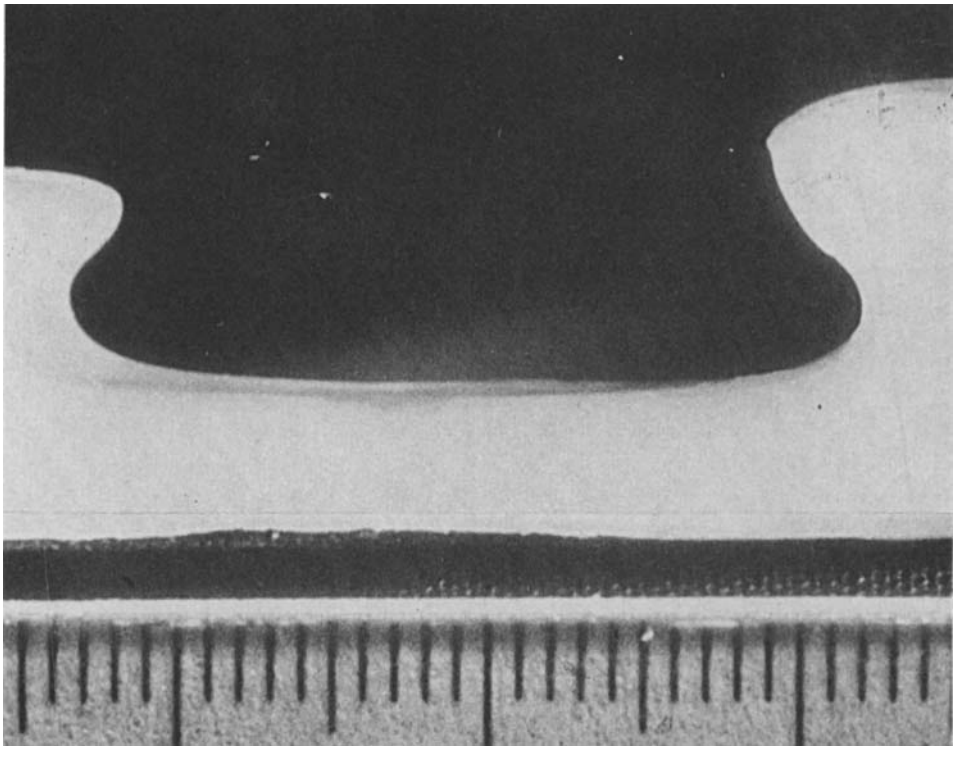

FIGURE 27. A cross-section of a thermal-erosion channel showing the undercut banks.

the current played an important role. The current tended to execute large-amplitude, cross-stream oscillations, as evidenced in figure 26 (*a*, *b*), before settling down to flow along a central channel. Flows with larger Reynolds numbers started to form well-developed channels by thermal erosion almost immediately, as seen in figure 26 (*c*, *d*), though some of the initial waviness was often preserved. The thermal-erosion rate quite clearly decreased monotonically with downstream distance, as seen in figure 26 (*d*), which is in qualitative agreement with the theoretical predictions. We did not, however, think it would be useful to carry out any quantitative comparisons, in part because the boundary condition at the top of the experimental gravity current was different from that of the theory.

Two effects occurred owing to the finite width of the current (in contrast to the infinite width of the theoretical model). First, an instability often developed in the flow whereby a slightly shallower region in the channel received less hot water flowing over it. This decreased the erosion rate, and hence accentuated the depth difference. This led to the formation of islands in the flow, as seen in figure 26 (*d*). Secondly, heat was lost from the current laterally as well as vertically, which led to the cross-sectional shape depicted in figure 27. The overhanging lip was protected from further melting as the flow level dropped beneath it. The determination of this shape consitutes a challenging and interesting free-boundary problem.

Geological consequences

The most extensively mapped area of komatiite flow is at Kambalda in Western Australia. The observations there show the komatiites now occupy long, linear

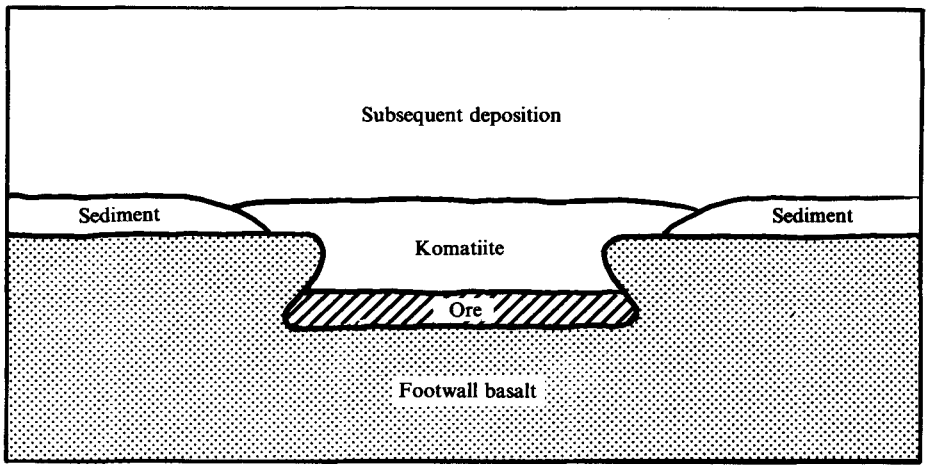

FIGURE 28. A simplified cross-section of the komatiite flow at Kambalda, Western Australia.

features, hundreds of metres below ground. Unaware of our work (as we were unaware of his), Lesher (1983) constructed a 'typical' cross-section from his many observations. A simplified version is reproduced in figure 28. The simplifications have been carried out only to highlight the essential aspects for those not expert in geology; a more geologically detailed version makes up figure 5.13 of Huppert & Sparks (1985). The agreement between the shape of the contact zone of the underlying basalt in this figure and the shape of the solid-wax boundary (figure 27) is remarkable. It strengthens the conclusion that the komatiite flowed out over a layer of sediment, melted it and then melted its way into the underlying basalt, just as modelled in the theory.

The aspect of komatiites that represents the greatest interest to an economic geologist is that they are the host to the major supply of the world's nickel. The ore, in the form of nickel sulphide, is often found at the base of komatiite flows. The explanation put forward by Huppert *et al.* (1984) and Huppert & Sparks (1985) is that nickel is present in very small concentrations in the original magma. As they flowed over the Earth's surface, the komatiites melted their way through sulphur-rich underlying rock and assimilated the melt. Nickel and sulphur have a great mutual affinity, so the sulphur attracted nickel to form fluid blobs of nickel sulphide, which are immiscible with, and considerably denser than, the molten lava (4.5 g cm^{-3} in contrast to 2.8 g cm^{-3}). The settling velocities of these blobs are such that, even in the vigorous, turbulent flow of the komatiite, they sink and form the ore layer depicted in figure 28.

From the model there follows an obvious 'working hypothesis' for exploratory drilling: if the core encounters old sediment, ore will not be found, so drilling of that (vertical) hole could be abandoned. This was exactly the 'rule of thumb' developed by the Western Mining Corporation after drilling approximately a thousand cores at Kambalda in the late 1960s.

6. Further problems

The few situations described above represent only a small fraction of those that make up GFM. An important additional area includes the dynamics of crystallization and, in particular, crystallization with induced compositional convection. This form

of convection arises because the composition of the crystals formed on cooling generally differs from that of the original fluid. Thus the fluid composition, and hence density, in the neighbourhood of the growing crystals is different from the far-field value. If the geometry allows it, this released liquid will convect.

In a study aimed at elucidating the fundamental principles of the dynamics of solidification, Huppert & Worster (1985) delineated the possible different flows when an initially homogeneous fluid with a simple phase diagram, such as a binary alloy, is cooled at a horizontal boundary. There are six different cases, because the cooling can be either from above or below, and the released liquid can be either relatively heavy (initial composition less than the eutectic value), relatively light (initial composition beyond the eutectic value) or of the same density, and composition, as the melt (of eutectic composition). Because of the different roles of the resulting thermal and compositional fields, each case involves different fluid-mechanical effects and a separate analysis. Huppert & Worster (1985) show how quantitative results for the rate of growth of the resultant crystal block can be obtained by the straightforward use of relationships for the conservation of heat and composition. They confined their particular calculations to the cases of cooling from below either an eutectic melt or a melt of subeutectic initial composition and obtained excellent agreement between their theoretical results and those obtained from laboratory experiments on aqueous solutions. Their general method has been applied to the other cases by Kerr (1984), Turner *et al.* (1986) and Huppert & Kerr (1986). The results derived by Turner *et al.* (1986) were then used to explain the final solidification of the komatiite lava flows discussed in §5. In particular, they were able to explain the characteristic fine-grained spinifex texture prevalent in the solid rock.

These sets of problems are basically one-dimensional, with horizontal variations that either are negligible or can be incorporated in some average sense. A more difficult situation occurs when crystallization is the result of cooling at a vertical wall. There are then necessarily horizontal temperature and compositional gradients which couple into the predominantly vertical flow of the cold, released fluid. At the moment, theoretical understanding of this area lags considerably behind the available experimental results. A detailed boundary-layer analysis has been conducted of the flow induced by a prescribed temperature and composition anomaly at a vertical wall in an unbounded fluid (Nilson & Baer 1982; Spera, Yuen & Kemp 1984; Nilson 1985; Nilson, McBirney & Baker 1985). Motivated by the geological context, these investigations concentrated on the case of positive density anomaly due to temperature, which would tend to induce downward motion, and negative density anomaly due to composition, which would tend to induce upward motion. Because the compositional diffusivity $D \ll \kappa_T \ll \nu$, where κ_T is the thermal diffusivity and ν is the kinematic viscosity, three regions can be discerned. In the inner region, closest to the wall, compositional buoyancy forces balance viscous forces. Beyond this, in the outer region, thermal buoyancy forces balance viscous forces. Finally, in the furthest region, the inner and outer motions are responded to by viscous coupling with the inertia forces. For given Prandtl number $Pr = \nu/\kappa_T$ and diffusivity ratio $\tau = D/\kappa_T$, the flow depends only on the ratio

$$\Gamma = \frac{\Delta\rho_T}{\Delta\rho_C} > 0, \tag{6.1a,b}$$

where $\Delta\rho_T$ and $\Delta\rho_C$ are the magnitudes of the prescribed density anomalies due to temperature and composition respectively. For sufficiently small (but positive) Γ, compositional effects overpower thermal effects; the entire flow is then upwards and

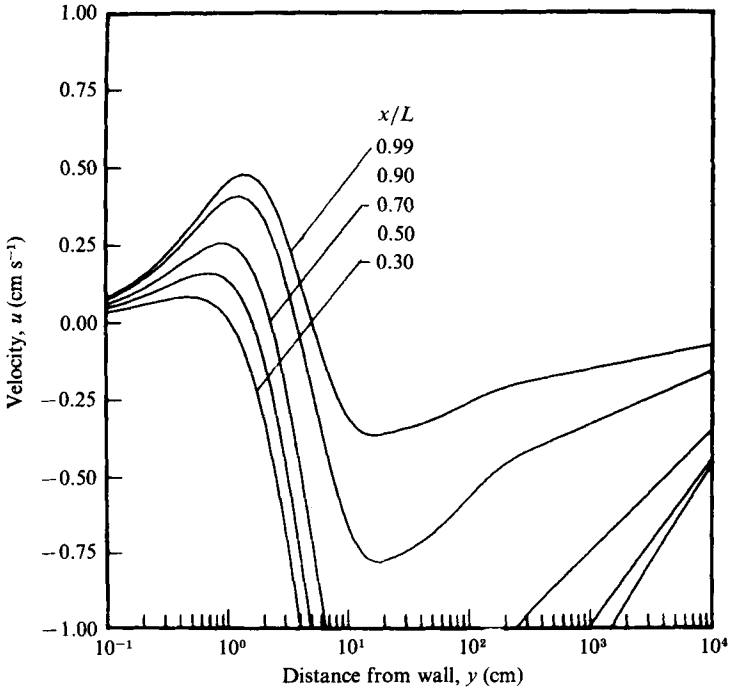

FIGURE 29. The vertical velocity as a function of distance from a wall of height L which maintains an increased composition and a decreased temperature over the far-field value. The profiles at five positions up the wall have been drawn using parameter values representative of basalt magmas from calculations reported by Nilson *et al.* (1985).

takes place in a boundary layer whose width increases like $x^{\frac{1}{4}}$, where x is the coordinate axis in the direction of flow. For sufficiently large Γ thermal effects dominate and the entire flow is downwards. For intermediate values of Γ, a bi-directional motion results, with an upwards inner flow and downwards outer flow. In the limit of large Pr, this occurs when $0.62\,\tau < \Gamma < 1.09\tau^{\frac{1}{3}}$ (Nilson 1985). On the further assumption that $\tau \ll 1$, Nilson matched an inner, upflowing boundary layer, whose width increases up the wall, to a very much thicker outer, downflowing boundary layer, whose width increases down the wall. A typical example of the resulting flow field, showing these regions with physical parameters corresponding to actual magmatic values, is presented in figure 29. The effects of flow through a crystal mush at the wall have also been modelled by supposing that the flow occurs in a porous medium (Lowell 1985).

The foregoing theoretical analysis has necessarily considered the ambient conditions to be unaltered. In a magma chamber of finite volume, and *a fortiori* in a small laboratory container, the boundary-layer flow alters the environment and is in turn altered by it; hence new phenomena can occur. These have begun to be investigated by a number of different groups (see, for example, McBirney 1980; Turner & Gustafson 1981; McBirney, Baker & Nilson 1985). But, at least in my opinion, there is still quite some way to go before a detailed quantitative understanding is obtained which can be applied with confidence to geological and other situations. Figure 30 (Plate 2) reproduces a photograph taken during one of Turner's experiments. A small, central rod was positioned in a solution of Na_2CO_3 that was initially almost saturated, and the rod was then cooled uniformly along its length. Crystals of $Na_2CO_3.10H_2O$

grew and released light liquid, which induced strong double-diffusive layering in the interior. Unanswered questions include: how can the rate of growth of the crystals be calculated; why is the thickness of the solid such a variable function of position along the rod; what governs the size of the double-diffusive layers formed; and why are there many thin ones at the top and thicker ones below?

An experimental study, which demonstrates many of the phenomena connected with crystallization, allows the cooling to take place at a sloping boundary and thus reproduces better the conditions found in magma chambers. By placing a slanted cooling plate in the interior of the fluid, an upward and downward surface can be investigated simultaneously and the differences easily conveyed (Huppert *et al.* 1986*a*). Figure 31 presents a sequence of photographs from one experiment. On both sides of the plate, crystallization releases light liquid. On the upper surface, this rises from where it was formed, as a series of plumes which mix with the environment and drive a large-scale flow. On the lower surface, the released liquid winds its way up through the crystal mush and is deposited at the top of the layer. As the temperature decreases so does the density of the released liquid, and it thus displaces fluid at the top of the layer downwards as in the familiar 'filling-box' problem (Baines & Turner 1969). These effects can be seen in figure 31 (*a*). As time proceeds, all the fluid in the region bounded by the downward-facing cooling surface finally reaches the eutectic composition. On the other side, double-diffusive layering with strong velocity gradients emerge, as seen in figure 31 (*b*).

The investigation of the melting of solid retaining walls by adjacent turbulent flows is another interesting topic, one aspect of which was considered in §5. Another aspect concerns the melting of a roof or floor of a container by an introduced hot fluid. We (Huppert, Sparks & Hallworth) have completed some experiments with a wax roof, whose initial thickness was about 15 cm, at the top of a Perspex container $20 \times 20 \times 40$ cm high. A hot aqueous solution was rapidly introduced near the base of the container until it was completely filled. The melting temperature of the PEG 1000 wax used is 37–40 °C and the initial temperature of the hot solution was around 70 °C. The density of the molten wax decreases fairly linearly between 1.11 g cm^{-3} at 40 °C to 1.09 g cm^{-3} at 70 °C. The density of the hot fluid could be varied by altering its concentration. Thus three separate cases could be considered. First, the fluid density could be less than the melt density (for all temperatures in the range 40–70 °C). The melt thus initially sank, but the turbulent motion resulting from the heat transfer to the cold roof quickly mixed the melt into the fluid. A photograph of a typical fluid/melt interface makes up figure 32 (*a*) (Plate 3). Secondly, the fluid density could exceed the melt density. In this case the melt formed a separate layer between the roof and the hot fluid. The layer was initially quiescent and transferred heat by conduction, though subsequently convection also occured. Figure 32 (*b*) (Plate 3) depicts a light melt layer that is in the latter state. Finally, an intermediate case is possible, in which the melt density at the melting point exceeds that of the hot fluid. The melt thus initially sank. As it did, its temperature rose and its density decreased to less than that of the fluid; streamers of melt subsequently rose. A photograph showing this bi-directional motion is reproduced in figure 32 (*c*) (Plate 3). A theoretical analysis of the first two cases has been completed.

Another general area of interest concerns the interaction between crystals, modelled as solid particles, and the fluid motions they are in. Geologists have been very influenced by Bowen (1928), who suggested that all crystals, once formed, settled out and were to be found at the bottom of the melt. This was questioned by Shaw (1965), McBirney & Noyes (1979) and also by Huppert & Sparks (1980*a*, *b*), who calculated

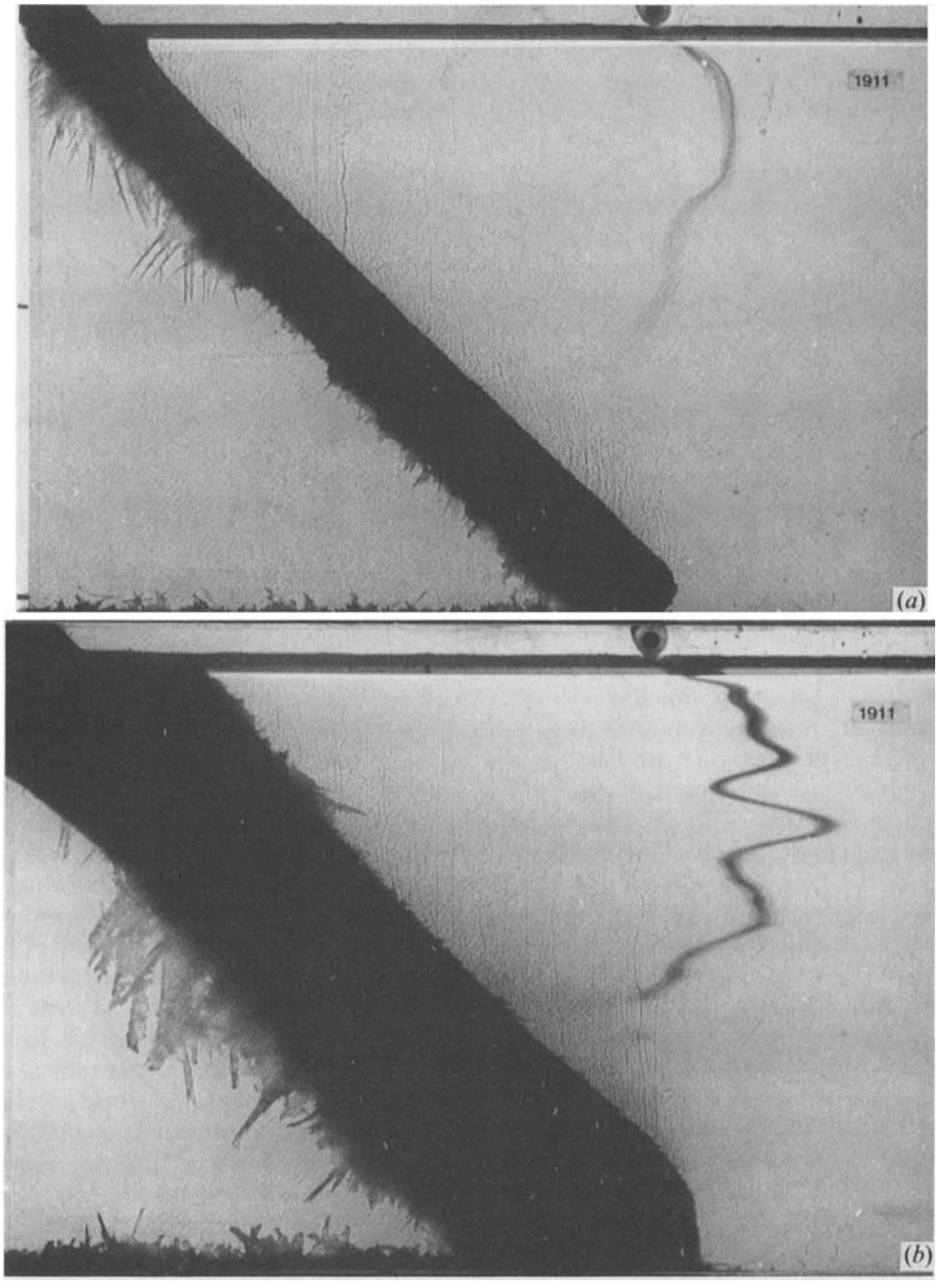

FIGURE 31. The result of cooling an initially homogeneous, almost saturated aqueous Na_2CO_3 solution at a 45° slope, (*a*) after 65 min, and (*b*) after 3.5 h. Note the very different forms of motion above and below the slope and the complex velocity structure above the slope in (*b*).

that high-Reynolds-number convective velocity fluctuations in a magma chamber greatly exceed the low-Reynolds-number free-fall speed of small (*c.* 1 mm) crystals, as described in §3. The crystals would thus remain suspended in the vigorous motion and grow in an environment correpsonding to the interior of the chamber. What happens when the fall velocity is in the range of the fluid velocity is not yet totally known. The idea (Stommel 1949) that heavy but small particles can be held in suspension in a steady, two-dimensional convective cell, has been extended by Marsh & Maxey (1985) to evaluate the fraction of crystals suspended in more general flow fields. The quantitative understanding of effects due to unsteady flow has been initiated by Smith & Spiegel (1985), who investigate how the spatial distribution of particles in an oscillatory convection cell change with time. They follow individual particle paths and equate the determined motion with the chaotic behaviour so frequently observed in studies of dynamical systems. Investigations of the effect of crystals on the motion itself are still awaited.

Magma viscosities can vary by orders of magnitude and yet magmas of different viscosities can mix, and mix quite intimately. In an interesting, fundamental study Campbell & Turner (1985, 1986) injected a heavy, turbulent axisymmetric 'fountain' of a low-viscosity fluid into a relatively lighter fluid of greater viscosity. They found that considerable mixing takes place, as the relatively heavy fluid in the fountain falls, only if the Reynolds number based on the input vertical velocity, source diameter and outer viscosity exceeds a value of about 70. They argue that only above this number are the turbulent eddies in the fountain able to engulf the viscous outer fluid. The mixing of fluid of greatly differing viscosities is without doubt an open field and has important applications to many situations of interest to geologists, chemical engineers and fluid dynamicists.

Volcanic plumes represent another area of considerable geological and fluid-mechanical interest. Figure 33 shows two of a sequence of photographs taken during the 1975 eruption of Ngauruhoe in New Zealand. The explosive eruption initiated a flow in excess of 400 m s^{-1} at the vent. When gas at a presssure of 3 bar was released into air at 1 bar, a shock wave was propagated through the atmosphere and rapidly caused condensation clouds to appear over the vent (figure 33*a*). The relatively heavy, hot ash ejecta rose from the vent as a momentum jet. The jet entrained ambient air around the edges, and the ash particles transferred part of their heat content to this air to make it positively buoyant, which increased the upward velocity of the outer parts of the jet. In the interior, which was virtually unaffected by the entrainment at the outer edges, heavy particles, especially the larger ones, began to fall and the column was divided into falling particles in the centre and rising particles at the edges (figure 33*a*). The rising part of the column continued to a height of approximately 8 km at an average speed of 12 m s^{-1}. The falling part formed a gravity current of hot, heavy particles in air, known as a pyroclastic flow, which raced down the slopes of the mountain. This flow also entrained ambient air and heated it, which caused part of the pyroclastic flow to separate from the slope and rise into the atmosphere (figure 33*b*).

This latter process has been simulated in the laboratory by continuously extruding a mixture of methanol and glycol (MEG) onto the underside of a slope in water (Huppert *et al.* 1986*b*). Mixtures of MEG and water can be heavier than either of the original components. Thus as the MEG current flows along the slope and entrains water, a relatively heavy mixture forms, which separates from the slope. Figure 34 reproduces a photograph of an experiment which has been inverted so that it is in

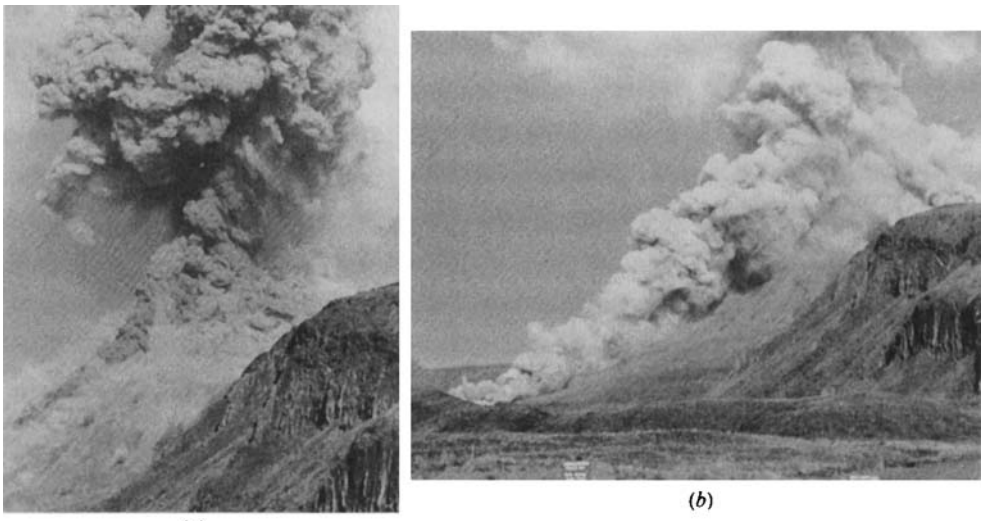

(*a*) (*b*)

FIGURE 33. The 1975 eruption of Ngauruhoe in New Zealand, photographed by G. T. Hancox. (*a*) 30 s and (*b*) 90 s after the initial explosive eruption.

the same orientation as the naturally occurring situation. The visual similarity between the flows in figures 33 (*b*) and 34 is striking.

On a larger geological scale, it has long been believed that most sinking slabs at island arcs descend to the phase discontinuity between the upper and lower mantle at 670 km (Isacks & Molnar 1971; Richter 1979). It is generally agreed that the slabs become compressed as they approach the discontinuity. Earthquakes are associated with the relative motion between the sinking slabs and the mantle, and none have ever been detected in the lower mantle (McKenzie & Richter 1976). While these facts are well accepted, the interpretation of them is very controversial at the moment. Current notions include suggestions that the slabs continue to propagate into the mantle (Creager & Jordan 1984, 1986), that they might lie along the discontinuity like an intruding gravity current at an interface (Richter & McKenzie 1978), that they might form giant megablobs because of the increased density below 670 km (Ringwood 1986), or that the material of the lower mantle is too hard and the viscosity contrast between the lower and upper mantle is too large ($\approx 10^{10}$) to allow any significiant interchange of matter across the discontinuity (McKenzie & Weiss 1975).

With this controversy in mind, Stewart Turner and I have conducted some preliminary experiments on axisymmetric viscous threads descending into viscous fluid layers. When a thin viscous thread falls onto a horizontal surface, it can become unstable at the base and oscillate either back and forth or in a circular fashion. It is believed that this behaviour is due to the thread being in compression at its end and buckling like an elastica. Taylor (1969) describes experiments designed to demonstrate this effect, and Buckmaster (1973) has considered some accompanying theoretical analysis. However, there is still much to be understood from a quantitative point of view, even though the effect is observed by many each morning at breakfast.

We carried out a series of experiments, and figure 35 (Plate 4) presents photographs

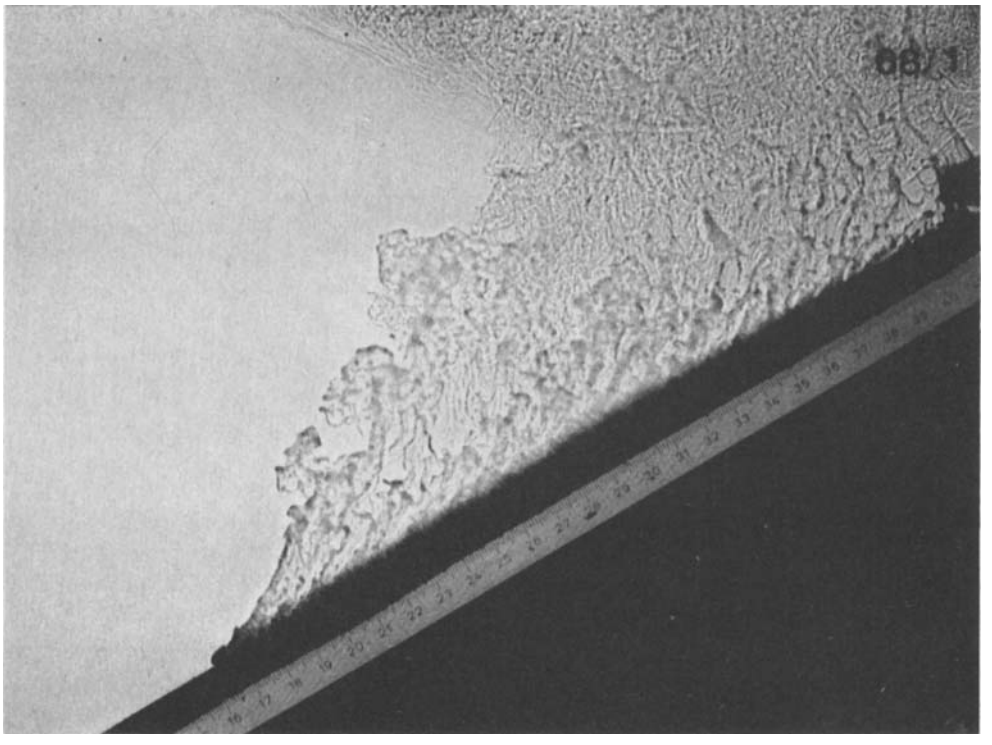

FIGURE 34. A mixture of methanol and ethylene glycol (MEG) issued from a point source onto an inclined plane in a large body of water. The entrained water mixes with the MEG to form a product which is more dense than either, and so it detaches from the slope and sinks. The photograph has been inverted so as to be directly comparable with the natural situation of figure 33(*b*).

of two of these. In the first (figure 35*a*), a glycerine thread at room temperature ($\rho \approx 1.26$ g cm^{-3} and $\nu \approx 12$ cm^2 s^{-1}) was allowed to descend into a 10.2 cm thick layer of water and glycerine ($\rho \approx 1.22$ g cm^{-3} and $\nu \approx 0.8$ cm^2 s^{-1}) above a heavier layer of less contaminated glycerine ($\rho \approx 1.25$ g cm^{-3} and $\nu \approx 5$ cm^{-2} s^{-1}). The thread oscillated at the free surface, as if the surface were solid, and these oscillations were carried down with remarkable regularity into the upper layer, as seen in figure 35(*a*). The second part of the figure shows the result of lowering the source point of the glycerine thread below the free surface. The instability is, of course, absent as the thread penetrates the upper layer. At the interface, however, it becomes unstable and the regular, oscillatory motion at the interface is carried down into the lower layer. The form of the motion in this layer differs from that depicted in figure 35(*a*) because here the instability occurs at an interface across which the density difference was rather small (≈ 0.02 g cm^{-3}), in contrast to the much larger density difference at the free surface. The figure also shows that fluid from the relatively light upper layer was dragged down by viscous coupling on the outside of the thread. It eventually rises because of its buoyancy, as can be seen in figure 35(*c*), which was taken some 12.5 min after figure 35(*b*). This figure also shows the spreading gravity current formed at the base of the container.

It is easy to envisage a number of different situations in which fluid of large viscosity flows into one, two or more layers of different fluid. For example, my student John Lister has calculated the rate of spreading of a viscous blob of fluid along an interface between two very viscous fluids. The motion within the fluid layers plays

a role in determining the rate of propagation of the intruding blobs and this makes the problem analytically difficult. Nevertheless, Lister (1986) has obtained theoretical results that agree well with experiments he has conducted.

The future?

I hope the foregoing has shown that there are many new areas of fluid mechanics that GFM is addressing. Because of the large range of different geological conditions, it is likely that many relevant fluid-mechanical concepts still need to be developed. Traditional geologists are beginning to learn about and incorporate the new fluid-mechanical possibilities and also beginning to suggest fluid-mechanical explanations of their own observations. All this, it seems to me, can only result in more research possibilities, as well as positions in geological organisations, for scientists with a knowledge of fluid flows. The amount of geological knowledge needed to contribute to GFM, however, suggests that individuals, who are trained generally in only one of the two disciplines of fluid mechanics or geology, may not find it easy to work by themselves. Teams of two or more complementary scientists, working with different skills on different aspects of problems, may become the norm. Nevertheless, I still believe that individual fluid dynamicists who are willing to read and understand a little of the geological background will derive enormous intellectual challenge, excitement and pleasure from the new problems that will arise.

The title of this paper was suggested to me by George Batchelor during one of our many fascinating conversations in which he has tried to instil 'the spirit of G. I. Taylor' into my research. It is a pleasure to thank my friend and colleague, Steve Sparks, who has selflessly spent many hours teaching me how geology can be exciting. Stewart Turner guided my first steps into both double-diffusive convection and laboratory experimentation; and I shall always be grateful to him. The writing of the paper was commenced during a visit to the University of New South Wales, Australia. I am grateful to the members of the School of Mathematics for the hospitality they provided during the period and for the financial support which made the visit possible, and to Dr and Mrs Sharota for the salubrious accommodation they organized. Mark Hallworth prepared many of the figures for publication and has greatly aided my experimental ventures during the last four years. The paper has been improved by helpful comments on earlier drafts by G. K. Batchelor, R. E. Britter, P. Bruce, R. C. Kerr, J. Lister, A. R. McBirney, D. P. McKenzie, B. D. Marsh, J. W. Miles, R. S. J. Sparks, J. S. Turner, J. A. Whitehead and M. G. Worster. My research is supported by grants from the BP Venture Research Unit and the NERC.

REFERENCES

BAINES, W. D. & TURNER, J. S. 1969 Turbulent buoyant convection from a source in a confined region. *J. Fluid Mech.* **37**, 51–80.

BOWEN, N. L. 1928 *The Evolution of the Igneous Rocks.* Princeton.

BRITTER, R. E. & LINDEN, P. F. 1980 The motion of the front of a gravity current travelling down an incline. *J. Fluid Mech.* **99**, 531–543.

BROWN, G. M. 1956 The layered ultrabasic rocks of Rhum, Inner Hebrides. *Phil. Trans. R. Soc. Lond.* B **240**, 1–53.

BUCKMASTER, J. 1973 The buckling of thin viscous jets. *J. Fluid Mech.* **61**, 449–463.

CAMPBELL, I. H. & TURNER, J. S. 1985 Turbulent mixing between fluids with different viscosities. *Nature* **313**, 39–42.

CAMPBELL, I. H. & TURNER, J. S. 1986 The influence of viscosity on fountains in magma chambers. *J. Petrol.* **27**, 1–30.

COLEMAN, R. G. & HOPSON, C. A. 1981 Oman Ophiolite. *J. Geophys. Res.* **86**, 2495–2782.

CRANFIELD, I. 1983 *Skiing down Everest and other Crazy Adventures.* Severn House.

CREAGER, K. C. & JORDAN, T. H. 1984 Slab penetration into the lower mantle. *J. Geophys. Res.* **89**, 3031–3049.

CREAGER, K. C. & JORDAN, T. H. 1986 Slab penetration into the lower mantle beneath the Mariama and other island arcs of the northwest Pacific. *J. Geophys. Res.* **91**, 3573–3589.

HOLMAN, J. P. 1976 *Heat Transfer.* McGraw-Hill.

HUPPERT, H. E. 1982*a* The propagation of two-dimensional and axisymmetric viscous gravity currents over a rigid horizontal surface. *J. Fluid Mech.* **121**, 43–58.

HUPPERT, H. E. 1982*b* Flow and instability of viscous gravity currents down a slope. *Nature* **300**, 427–429.

HUPPERT, H. E. & KERR, R. C. 1986 Solidifying from below an initially homogeneous solution whose composition exceeds the eutectic, with particular application to an NH_4Cl solution. *J. Fluid Mech.* (submitted).

HUPPERT, H. E., KERR, R. C. & SPARKS, R. S. J. 1984 Notes on supersaturation. Unpublished paper.

HUPPERT, H. E., SHEPHERD, J. B., SIGURDSSON, H. & SPARKS, R. S. J. 1982*a* On lava dome growth, with applications to the 1979 lava extrusion of Soufrière, St Vincent. *J. Volcanol. Geotherm. Res.* **14**, 199–222.

HUPPERT, H. E. & SPARKS, R. S. J. 1980*a* Restrictions on the compositions of mid-ocean ridge basalts: a fluid dynamical investigation. *Nature* **286**, 46–48.

HUPPERT, H. E. & SPARKS, R. S. J. 1980*b* The fluid dynamics of a basaltic magma chamber replenished by influx of hot, dense ultrabasic magma. *Contrib. Mineral. Petrol.* **75**, 279–289.

HUPPERT, H. E. & SPARKS, R. S. J. 1984 Double-diffusive convection due to crystallization in magmas. *Ann. Rev. Earth Planet. Sci.* **12**, 11–37.

HUPPERT, H. E. & SPARKS, R. S. J. 1985 Komatiites I: Eruption and flow. *J. Petrol.* **26**, 694–725.

HUPPERT, H. E., SPARKS, R. S. J. & TURNER, J. S. 1982*b* The effects of volatiles on mixing in calcalkaline magma systems. *Nature* **297**, 554–557.

HUPPERT, H. E., SPARKS, R. S. J. & TURNER, J. S. 1983 Laboratory investigations of viscous effects in replenished magma chambers. *Earth Planet. Sci. Lett.* **65**, 377–381.

HUPPERT, H. E., SPARKS, R. S. J. & TURNER, J. S. 1984 Some effects of viscosity on the dynamics of replenished magma chambers. *J. Geophys. Res.* **89**, 6857–6877.

HUPPERT, H. E., SPARKS, R. S. J., TURNER, J. S. & ARNDT, N. T. 1984 Emplacement and cooling of komatiite lavas. *Nature* **309**, 19–22.

HUPPERT, H. E., SPARKS, R. S. J., WILSON, J. R. & HALLWORTH, M. A. 1986*a* Cooling and crystallization at an inclined plane. *Earth Planet. Sci. Lett.* **79**, 319–328.

HUPPERT, H. E. & TURNER, J. S. 1981 A laboratory model of a replensihed magma chamber. *Earth Planet. Sci. Lett.* **54**, 144–152.

HUPPERT, H. E., TURNER, J. S., CAREY, S. N., SPARKS, R. S. J. & HALLWORTH, M. A. 1986*b* A laboratory simulation of pyroclastic flows down slopes. *J. Volcanol. Geotherm Res.* (in press).

HUPPERT, H. E., TURNER, J. S. & SPARKS, R. S. J. 1982*c* Replenished magma chambers: effects of compositional zonation and input rates. *Earth Planet. Sci. Lett.* **57**, 345–357.

HUPPERT, H. E. & WORSTER, M. G. 1985 Dynamic solidification of a binary melt. *Nature* **314**, 703–707.

ISACKS, B. & MOLNAR, P. 1971 Distribution of stresses in the descending lithosphere from a global survey of focal-mechanism solutions of mantle earthquakes. *Rev. Geophys. Space Phys.* **9**, 103–174.

KERR, R. C. 1984 Crystallization and compositional convection in geological fluid mechanics. Ph.D. thesis, University of Cambridge, England.

KIEFFER, S. W. 1977 Sound speed in liquid–gas mixtures: water–air and water–steam. *J. Geophys. Res.* **82**, 2895–2904.

LESHER, C. M. 1983 Localisation and genesis of Fe–Ni–Cu sulphide mineralisation at Kambalda, Western Australia, Ph.D. thesis. University of Western Australia.

LISTER, J. R. 1986 The intrusion of a gravity current along an interface between two viscous fluids. *J. Fluid Mech.* (submitted).

LOWELL, R. P. 1985 Double-diffusive convection in partially molten silicate systems: its role during magma production and in magma chambers. *J. Volcanol. Geotherm Res.* **26**, 1–24.

MCBIRNEY, A. R. 1980 Mixing and unmixing of magmas. *J. Volcanol. Geotherm. Res.* **7**, 357–371.

MCBIRNEY, A. R., BAKER, B. H. & NILSON, R. H. 1985 Liquid fractionation. Part I: basic principles and experimental simulations. *J. Volcanol. Geotherm. Res.* **24**, 1–24.

MCBIRNEY, A. R. & MURASE, T. 1984 Rheological properties of magmas. *Ann. Rev. Earth Planet. Sci.* **12**, 337–357.

MCBIRNEY, A. R. & NOYES, R. M. 1979 Crystallization and layering of the Skaergaard intrusion. *J. Petrol.* **20**, 483–554.

MCKENZIE, D. P. 1984 The generation and compaction of partially molten rock. *J. Petrol.* **25**, 713–765.

MCKENZIE, D. P. 1985 The extraction of magma from the crust and mantle. *Earth Planet. Sci. Lett.* **74**, 81–91.

MCKENZIE, D. P. & RICHTER, F. M. 1976 Convective currents in the earth's mantle. *Sci. Am.* **235**, 72–89.

MCKENZIE, D. P. & WEISS, N. O. 1975 Speculations on the thermal and tectonic history of the earth. *Geophys. J. R. Astron. Soc.* **42**, 131–174.

MARSH, B. D. 1978 On the cooling of ascending andesitic magma. *Phil. Trans. R. Soc. Lond.* A **288**, 611–625.

MARSH, B. D. 1981 On the crystallinity, probability of occurrence and rheology of lava and magma. *Contrib. Mineral. Petrol.* **78**, 85–98.

MARSH, B. D. & MAXEY, M. R. 1985 On the distribution and separation of crystals. *J. Volcanol. Geotherm. Res.* **24**, 95–150.

MURASE, T. & MCBIRNEY, A. R. 1973 Properties of some common igneous rocks and their melts at high temperatures. *Geol. Soc. Am. Bull.* **84**, 3563–3592.

NELSON, S. A. & CARMICHAEL, I. S. E. 1979 Partial molar volumes of oxide components in silicate liquids. *Contrib. Mineral Petrol.* **71**, 117–124.

NILSON, R. H. 1985 Countercurrent convection in a double-diffusive boundary layer. *J. Fluid Mech.* **160**, 181–210.

NILSON, R. H. & BAER, M. R. 1982 Double-diffusive counterbuoyant boundary layer in laminar natural convection. *Intl J. Heat Mass Transfer* **25**, 285–287.

NILSON, R. H., MCBIRNEY, A. R. & BAKER, B. H. 1985 Liquid fractionation. Part II: fluid dynamics and quantitative implications for magmatic systems. *J. Volcanol. Geotherm. Res.* **24**, 25–54.

RAEDEKE, L. D. & MCCALLUM, I. S. 1984 Investigations in the Stillwater complex. Part II. Petrology and petrogenesis of the ultramafic series. *J. Petrol.* **25**, 395–420.

RICHTER, F. M. 1979 Focal mechanisms and seismic energy release of deep and intermediate earthquakes in the Tonga–Kermadec region and their bearing on the depth extent of mantle flow. *J. Geophys. Res.* **84**, 6783–6795.

RICHTER, F. M. & MCKENZIE, D. P. 1978 Simple plate models of mantle convection. *J. Geophys. Res.* **44**, 441–471.

RICHTER, F. M. & MCKENZIE, D. P. 1984 Dynamical models for melt segregation from a deformable matrix. *J. Geol.* **92**, 729–740.

RINGWOOD, A. E. 1986 Dynamics of subducted lithosphere and implications for basalt petrogenesis. *Terra cognita.* **6**, 67–77.

SCOTT, D. R. & STEVENSON, D. J. 1984 Magma solitons. *Geophys. Res. Lett.* **11**, 1161–1164.

SCOTT, D. R., STEVENSON, D. J. & WHITEHEAD, J. A. 1986 Observations of solitary waves in a viscously deformable pipe. *Nature* **319**, 759–761.

SHAW, H. R. 1965 Comments on viscosity, crystal settling, and convection in granitic magmas. *Am. J. Sci.* **263**, 120–152.

SHAW, H. R. 1969 Rheology of basalt in the melting range. *J. Petrol.* **10**, 510–535.

SILVI, N. & DUSSAN V., E. B. 1985 On the rewetting of an inclined solid surface by a liquid. *Phys. Fluids* **28**, 5–7.

SIMPSON, J. E. & BRITTER, R. E. 1979 The dynamics of the head of a gravity current advancing over a horizontal surface. *J. Fluid Mech.* **94**, 477–495.

SMITH, L. A. & SPIEGEL, E. A. 1985 Pattern formation by particles settling in viscous flows. *Columbia University Astronomy and Astrophysics Preprint No.* A67.

SPARKS, R. S. J. 1986 The dimensions and dynamics of volcanic eruption columns. *Bull. Volcanol.* **48**, 3–15.

SPARKS, R. S. J. & HUPPERT, H. E. 1984 Density changes during the fractional crystallization of basaltic magmas: implications for the evolution of layered intrusions. *Contrib. Mineral. Petrol.* **85**, 300–309.

SPARKS, R. S. J., HUPPERT, H. E. & TURNER, J. S. 1984 The fluid dynamics of evolving magma chambers. *Phil. Trans. R. Soc. Lond.* A **310**, 511–534.

SPENCE, D. A. & TURCOTTE, D. L. 1985 Magma-driven propagation of cracks. *J. Geophys. Res.* **90**, 575–580.

SPENCE, D. A., SHARP, P. W. & TURCOTTE, D. L. 1986 Buoyancy driven crack propagation: a mechanism for magma migration. *J. Fluid Mech.* **174**, 135–153.

SPERA, F. J., YUEN, D. A. & KEMP, D. V. 1984 Mass transfer rates along vertical walls in magma chambers and marginal upwelling. *Nature* **310**, 764–767.

STOMMEL, H. 1949 Trajectories of small bodies sinking slowly through convection cells. *J. Mar. Res.* **8**, 24–29.

TAIT, S. R. 1985 Fluid dynamic and geochemical evolution of cyclic unit 10, Rhum, Eastern Layered Series. *Geol. Mag.* **122**, 469–484.

TAYLOR, G. I. 1969 Instability of jets, threads, and sheets of viscous fluid. In *Proc. 12th Intl Congress of Appl. Mech. Stanford, 1968*, pp. 382–388. Springer.

TURNER, J. S. & GUSTAFSON, L. B. 1981 Fluid motions and compositional gradients produced by crystallization or melting at vertical boundaries. *J. Volcanol. Geotherm. Res.* **11**, 93–125.

TURNER, J. S., HUPPERT, H. E. & SPARKS, R. S. J. 1983 Experimental investigations of volatile exsolution in evolving magma chambers. *J. Vocanol. Geotherm. Res* **16**, 263–277.

TURNER, J. S., HUPPERT, H. E. & SPARKS, R. S. J. 1986 Komatiites II: Experimental and theoretical investigations of post-emplacement cooling and crystallization. *J. Petrol.* **27**, 397–437.

WASHBURN, E. D. 1929 *International Critical Tables.* McGraw-Hill.

WESTERCAMP, D. & TOMBLIN, J. F. 1979 Le volcanisme récent et les éruptions historique dans la partie centrale de l'arc insulaire des petites Antilles. *Bull. BGRM* (deuxieme serie) Section IV n. 3/4, 293–319.

WILSON, L., SPARKS, R. S. J. & WALKER, G. P. L. 1980 Explosive volcanic eruptions – IV. The control of magma properties and conduit geometry on eruption column behaviour. *Geophys. J. R. Astron. Soc.* **63**, 117–148.